The evolution of Lyman-break galaxies in CDM

C. G. Lacey $\star$,[1] C. M. Baugh,[1] C.S. Frenk,[1] A.J. Benson[2]

[1]*Institute for Computational Cosmology, Department of Physics, University of Durham, South Road, Durham, DH1 3LE, UK*
[2]*Mail Code 130-33, California Institute of Technology, Pasadena, CA 91125, USA*

17 November 2010

ABSTRACT
We make a detailed investigation of the properties of Lyman-break galaxies (LBGs) in the
ΛCDM model. We present predictions for two published variants of the GALFORM semi-
analytical model: the Baugh et al. (2005) model, which has star formation at high redshifts
dominated by merger-driven starbursts with a top-heavy IMF, and the Bower et al. (2006)
model, which has AGN feedback and a standard Solar neighbourhood IMF throughout. We
show predictions for the evolution of the rest-frame far-UV luminosity function in the red-
shift range $z = 3 - 20$, and compare with the observed luminosity functions of LBGs at
$z = 3 - 10$. We find that the Baugh et al. model is in excellent agreement with these observa-
tions, while the Bower et al. model predicts too many high-luminosity LBGs. Dust extinction,
which is predicted self-consistently based on galaxy gas contents, metallicities and sizes, is
found to have a large effect on LBG luminosities. We compare predictions for the size evo-
lution of LBGs at different luminosities with observational data for $2 \lesssim z \lesssim 7$, and find the
Baugh et al. model to be in good agreement. We present predictions for stellar, halo and gas
masses, star formation rates, circular velocities, bulge-to-disk ratios, gas and stellar metal-
licities and clustering bias, as functions of far-UV luminosity and redshift. We find broad
consistency with current observational constraints. We then present predictions for the abun-
dance and angular sizes of LBGs out to very high redshift ($z \leqslant 20$), finding that planned
deep surveys with *JWST* should detect objects out to $z \lesssim 15$. We predict that the effects of
dust extinction on the far-UV luminosity density should be large (~ 2 mag), even out to high
redshifts. The typical UV luminosities of galaxies are predicted to be very low at high red-
shifts, which has implications for detecting the galaxies responsible for reionizing the IGM;
for example, at $z = 10$, 50% of the ionizing photons are expected to be produced by galaxies
fainter than $M_{\rm AB}(1500\text{Å}) - 5\log h \sim -15$.

Key words: galaxies: evolution – galaxies: formation – galaxies: high-redshift

1 INTRODUCTION

The discovery of Lyman-break galaxies at $z \sim 3$ by Steidel et al.
(1996) was a breakthrough in observational studies of galaxy for-
mation. It provided, for the first time, a significant sample of normal
galaxies at high redshift whose properties and population statistics
could then be investigated observationally and compared to the pre-
dictions of theoretical models (Baugh et al. 1998).

   Lyman-break galaxies (LBGs) are star-forming galaxies
which are identified through the Lyman-break feature in their
spectra. This feature is produced by absorption by neutral hy-
drogen in the atmospheres of massive stars, in the interstellar
medium (ISM) of the galaxy and in the intergalactic medium (IGM)
(Steidel & Hamilton 1992). For ground-based observations, detec-
tion of the Lyman break is restricted to redshifts $z \gtrsim 3$. Since the
first successful demonstration by Steidel et al. (1996) at $z \sim 3$,
the technique has been extended to identify galaxies at both higher

redshifts and lower luminosities, using ground-based telescopes
and the Hubble Space Telescope (HST) (e.g. Madau et al. 1996;
Steidel et al. 1999; Bouwens et al. 2003; Shimasaku et al. 2005;
Yoshida et al. 2006). Finding LBGs at $z \gtrsim 6$ requires observing
in the near-IR, which was first done using NICMOS on HST, and
led to the identification of a small number of $z \sim 7 - 8$ objects
(Bouwens et al. 2004b). More recently, the WFC3/IR camera on
HST has allowed the discovery of much larger samples of LBGs at
$z \sim 7 - 8$ (Bouwens et al. 2010; McLure et al. 2010; Oesch et al.
2010b; Bunker et al. 2009; Yan et al. 2009) and even a few candi-
dates at $z \sim 10$ (Bouwens et al. 2009b). By observing in the UV
from space, the *GALEX* satellite has also been used to find LBGs at
$z \sim 1$ (Burgarella et al. 2006).

   Follow-up observational investigations on LBGs have in-
cluded estimates of their star formation rates (SFRs), sizes, mor-
phologies, stellar and dynamical masses, galactic outflows, metal-
licities, dust extinctions, gas masses, IR/sub-mm emission from
dust and clustering (Steidel et al. 1996; Giavalisco et al. 1996;
Adelberger et al. 1998; Chapman et al. 2000; Pettini et al. 2001;

$\star$ E-mail: Cedric.Lacey@durham.ac.uk (CGL)

Shapley et al. 2001; Ferguson et al. 2004). Since LBGs are selected on the basis of their rest-frame far-UV emission, which is dominated by massive young stars, LBG samples at different redshifts also provide a means to trace the cosmic star formation history, a key component in our picture of galaxy formation (Madau et al. 1996), although important uncertainties remain due to the effects of dust extinction. Observations of LBGs at $z = 3 - 10$ probe galaxy evolution over the first 3–15% of the age of the universe.

Other observational techniques have also been used to find normal galaxies at high redshift. Searches for star-forming galaxies via their Lyα emission line (e.g. Hu et al. 1998) cover a similar redshift range to LBGs. The main drawback with this technique is that some star forming-galaxies show Lyα absorption rather than emission (Shapley et al. 2003), and consequently are missed in narrowband surveys. A further complication is that inferring the SFR from the Lyα emission line is much more uncertain than inferring it from the far-UV continuum, since the effects of dust extinction are amplified by resonant scattering of Lyα photons by hydrogen atoms. Another technique is to search for sub-mm or IR emission from dust in high-z star-forming galaxies (Smail et al. 1997; Hughes et al. 1998). This method is currently limited by source confusion at faint fluxes due to the relatively poor angular resolution of current IR/sub-mm telescopes, which restricts searches to redshifts $z \lesssim 3$ and mostly to the galaxies with the highest SFRs. Other techniques for selecting high-z galaxies, which are sensitive also to non-star-forming galaxies (such as ERO and DRG colour selection) are limited to even lower redshifts $z \lesssim 2$. Overall, the Lyman-break technique still seems the most effective for finding large samples of star-forming galaxies at $z \gtrsim 3$ that cover a wide range of luminosities and SFRs.

The theoretical significance of the discovery of LBGs was highlighted early on using semi-analytical models of galaxy formation. Baugh et al. (1998) showed that the abundance and observed properties of the $z \sim 3 - 4$ LBGs found by Steidel et al. (1996) and Madau et al. (1996) could be explained in the framework of CDM, and that they fitted into a picture in which the cosmic SFR density peaked around a redshift $z \sim 2$. This evolution of the cosmic SFR density was driven by the combined effects of the build-up of dark matter halos, gas cooling and supernova feedback. Their model had star formation occuring mostly in quiescent disks, and neglected the effects of dust extinction. Subsequent observational studies found evidence from UV continuum slopes for significant dust extinction in LBGs (Meurer et al. 1999; Steidel et al. 1999). Somerville et al. (2001) proposed a different semi-analytical model in which star formation bursts triggered by galaxy mergers played an important role, and combined this with an empirical prescription for dust extinction, tuned to match observational estimates of the extinction for $z \sim 3$ LBGs.

More recent studies of LBGs in semi-analytical models include Guo & White (2009) and Lo Faro et al. (2009), which investigated the effects on inferred luminosity functions and other properties of applying observational LBG colour selections to model galaxies. The former used a phenomenological model for dust extinction, while the latter used a physical model similar to that in the present paper. LBGs were also studied in gas-dynamical simulations of galaxy formation (Nagamine 2002; Weinberg et al. 2002), but these simulations had the drawback that they did not predict properties for the present-day galaxy population consistent with observations, unlike the semi-analytical models. Furthermore, none of these models were able to explain the number counts and redshifts of faint sub-mm galaxies discovered in surveys at $850\mu m$

(Smail et al. 1997), which were subsequently shown to be dusty starbursts at $z \sim 2 - 3$ (Chapman et al. 2003).

In order to explain within a single framework the sub-mm and Lyman-break galaxies at high redshift, together with a wide range of galaxy properties at $z = 0$ (including optical and near- and far-IR luminosity functions, gas fractions, metallicities and galaxy sizes), Baugh et al. (2005) introduced a new semi-analytical model in which the gas consumption timescale in disks at high redshifts was increased, with the result that starbursts triggered by galaxy mergers played a more significant role at high redshift. They assumed, further, that stars formed in these bursts with a top-heavy initial mass function (IMF). Unlike previous models of high-redshift galaxies, this model included a fully self-consistent treatment of both absorption and emission of radiation by dust, with dust extinction calculated from radiative transfer based on the predicted gas masses, metallicities and sizes of galaxies, and the spectrum of the dust emission calculated by solving for the temperature distribution of the dust grains in each galaxy. In subsequent papers, we have explored other predictions from the same model, including stellar and gas metallicities (Nagashima et al. 2005a,b), galaxy colours, sizes and morphologies in the local universe (Almeida et al. 2007; González et al. 2009), the evolution of Lyα-emitters (Le Delliou et al. 2005, 2006; Orsi et al. 2008), and the evolution of galaxies at mid- and far-IR wavelengths (Lacey et al. 2008, 2010b), finding generally good agreement with observational data.

In Baugh et al. (2005), we made only a limited comparison with observational data on LBGs, focussing on their rest-frame far-UV luminosity function at $z = 3$. Since then, there has been a huge increase in the amount and quality of observational data on LBGs, in particular enabling measurements of the luminosity function of LBGs out to $z \sim 10$. Therefore in this paper we return to studying LBGs, making detailed predictions for the evolution of their luminosity functions over a wide redshift range ($z = 3 - 20$) and for many other properties. We consider two variants of the GALFORM semi-analytical model (Cole et al. 2000), those of Baugh et al. (2005) and Bower et al. (2006). The two models differ in a number of significant ways, the most important being that the Bower et al. model includes AGN feedback, while the Baugh et al. model has a variable IMF, as already mentioned. We focus here on far-UV-selected galaxies in the redshift range $z \gtrsim 3$, where they are observationally detected using their Lyman-break features. We investigate the present-day descendants of LBGs in a companion paper (Gonzalez et al. 2010a), and make predictions for the reionization of the IGM from the same models in Raičević et al. (2010a,b). The properties and evolution of far-UV-selected galaxies at lower redshifts will be the topic of a separate paper.

The plan of this paper is as follows: In §2, we briefly review the main features of the two models. In §3, we compare predictions for the evolution of the far-UV luminosity function with observational data from LBGs, and investigate the sensitivity of these predictions to various model parameters. In §4, we investigate the sizes and other physical properties of UV-selected galaxies, and carry out a detailed comparison with the observed sizes of LBGs. In §5, we present predictions for LBGs at very high redshifts, which may be accessible with future telescopes such as *JWST* and ELTs. In §6, we show how our predictions for LBGs fit into the wider picture of the evolution of the cosmic star formation and UV luminosity densities. We briefly consider the contribution of LBGs to the reionization of the IGM. Finally, we present our conclusions in §7.

2 THE GALFORM GALAXY FORMATION MODEL

We compute the formation and evolution of galaxies within the framework of the ΛCDM model of structure formation using the semi-analytical galaxy formation model GALFORM. The general methodology and approximations behind GALFORM are set out in detail in Cole et al. (2000) (see also the review by Baugh 2006). In summary, GALFORM follows the main processes which shape the formation and evolution of galaxies. These include: (i) the collapse and merging of dark matter halos; (ii) the shock-heating and radiative cooling of gas inside dark halos, leading to the formation of galaxy disks; (iii) quiescent star formation in galaxy disks; (iv) feedback from supernova explosions, from AGN heating, and from photoionization of the IGM; (v) chemical enrichment of the stars and gas; (vi) galaxy mergers driven by dynamical friction within common dark matter halos, leading to the formation of stellar spheroids, and also triggering bursts of star formation. The end product of the calculations is a prediction of the numbers and properties of galaxies that reside within dark matter haloes of different masses. The model predicts the stellar and cold gas masses of the galaxies, along with their star formation and merger histories, their disk and bulge sizes, and their metallicities. The stellar luminosities of the galaxies are then computed from their star formation and chemical enrichment histories using a stellar population model. Finally, the dust extinctions at different wavelengths are calculated self-consistently from their gas and metal contents and sizes using a radiative transfer model.

2.1 Baugh05 and Bower06 models

The two variants of GALFORM considered in this paper, Baugh et al. (2005) and Bower et al. (2006) (hereafter Baugh05 and Bower06), have been used as fiducial models in a number of investigations. We now briefly compare the main features of the two models. Similar discussions can be found in Almeida et al. (2007, 2008), González et al. (2009) and Gonzalez-Perez et al. (2009). For full details of the two models, see the papers by Cole et al. (2000), Baugh et al. (2005) (also Lacey et al. (2008)), and Bower et al. (2006). We give a summary of previously published results obtained with the two models, and of their relative performances in explaining different observed properties of galaxies, in the Appendix.

(i) *Cosmology:* The Baugh05 model adopts a ΛCDM cosmology with a present-day matter density parameter, $\Omega_m = 0.3$, a cosmological constant, $\Omega_\Lambda = 0.7$, a baryon density, $\Omega_b = 0.04$, a Hubble constant $h = 0.7$ in units of $100 \mathrm{km\,s^{-1}Mpc^{-1}}$, and a power spectrum normalization given by $\sigma_8 = 0.93$. The Bower06 model instead uses the cosmological model assumed in the Millennium simulation (Springel et al. 2005), where $\Omega_m = 0.25$, $\Omega_\Lambda = 0.75$, $\Omega_b = 0.045$, $h = 0.73$ and $\sigma_8 = 0.9$.

(ii) *Star formation in disks:* In both models, stars can form either quiescently in disks or in starbursts at a rate $\psi = M_{\mathrm{gas}}/\tau_*$, where M_{gas} is the mass of cold gas and the timescale, τ_*, is different in disks and bursts. The two models adopt different parameterizations for the dependence of the quiescent timescale on disk properties. In the Baugh05 model, this timescale varies simply as a power of the disk circular velocity, while in the Bower06 model it is proportional also to the disk dynamical time. Since the typical dynamical time gets shorter with increasing redshift, the star formation timescale in the Bower06 model is shorter at high redshift than it would be in the equivalent disk in the Baugh05 model. As a consequence, galactic disks at high redshift tend to be gas poor in the Bower06 model, but gas rich in the Baugh05 model. This then results in much more gas being available to fuel starbursts and in a higher fraction of star formation occuring in bursts at high redshift in the Baugh05 compared to the Bower06 model.

(iii) *Starbursts:* In the Baugh05 model, starbursts are triggered only by galaxy mergers (both major and minor), while in the Bower06 model, starbursts are triggered also by disk instabilities. (We define major mergers as those in which the mass ratio of the smaller to larger galaxy exceeds 0.3.) Both major mergers and disk instabilities are assumed to transform the stellar disk(s) into a spheroid, while in minor mergers only the stars from the smaller galaxy are added to the spheroid, leaving the stellar disk of the larger galaxy intact. Stars formed in bursts are always added to the spheroid. The star formation timescale in bursts is assumed to be

$$\tau_{*\mathrm{burst}} = \max[f_{\mathrm{dyn}}\tau_{\mathrm{dyn}}, \tau_{*\mathrm{burst,min}}], \qquad (1)$$

so that it scales with the spheroid dynamical time τ_{dyn}, but with a "floor" value when this is very short. The parameters f_{dyn} and $\tau_{*\mathrm{burst,min}}$ are different in the two models: $f_{\mathrm{dyn}} = 50$ and $\tau_{*\mathrm{burst,min}} = 0.2\mathrm{Gyr}$ in the Baugh05 model and $f_{\mathrm{dyn}} = 2$ and $\tau_{*\mathrm{burst,min}} = 0.005\mathrm{Gyr}$ in the Bower06 model, so that the burst SFR timescale is 25-40 times larger in the Baugh05 model compared to the equivalent galaxy in the Bower06 model. The SFR in a burst then decays exponentially with time, with a timescale that depends on the supernova feedback efficiency and gas recycling fraction as well as the SFR timescale. The burst is assumed to be truncated after n_τ e-folding times, at which point the remaining gas in the burst is ejected into the halo (see Granato et al. (2000) for more details). The Baugh05 and Bower06 models both assume $n_\tau = 3$.

(iv) *Stellar initial mass function (IMF):* The Bower06 model uses the Kennicutt (1983) IMF, consistent with deductions from the Solar neighbourhood, in all modes of star formation. This has the form $\mathrm{d}N/\mathrm{d}\ln m \propto m^{-x}$ (where N is the number of stars and m is the stellar mass) with slope $x = 0.4$ for $m < M_\odot$ and $x = 1.5$ for $m > M_\odot$ (compared to $x = 1.35$ for the Salpeter IMF). The Baugh05 model also adopts this IMF in quiescent star formation in galactic disks. However, in starbursts triggered by galaxy mergers, a top-heavy IMF is assumed, with slope $x = 0$. The IMF covers the stellar mass range $0.15 < m < 120M_\odot$ in all cases. The yield of metals (p) and the fraction of gas recycled per unit mass of stars formed (R) are chosen to be consistent with the form of the IMF. We assume $p = 0.023$ and $R = 0.41$ for the Kennicutt IMF, and $p = 0.15$ and $R = 0.91$ for the top-heavy $x = 0$ IMF.

(v) *Supernova (SN) feedback:* In both models, supernova explosions are assumed to reheat cold gas (in both disks and starbursts) and eject it into the halo, at a rate

$$\dot{M}_{\mathrm{eject}} = (V_{\mathrm{hot}}/V_{\mathrm{gal}})^{\alpha_{\mathrm{hot}}}\psi, \qquad (2)$$

where V_{gal} is the circular velocity of the disk (for quiescent star formation) or spheroid (for bursts), and V_{hot} and α_{hot} are parameters. The SN feedback is much stronger in the Bower06 model ($V_{\mathrm{hot}} = 485\mathrm{kms^{-1}}$ and $\alpha_{\mathrm{hot}} = 3.2$, compared with $V_{\mathrm{hot}} = 300\mathrm{kms^{-1}}$ and $\alpha_{\mathrm{hot}} = 2$ in the Baugh05 model). A further difference is that in the Bower06 model ejected gas is reincorporated into the halo on a shorter timescale than in the Baugh05 model. This SN feedback supresses star formation much more effectively in low mass than high mass galaxies.

(vi) *Superwind vs AGN feedback:* A major difference between the two models is in the modelling of feedback in massive galaxies. If only the "standard" SN feedback described above is included, then too much gas cools in massive halos, resulting in the break

at the bright end of the present-day optical and near-IR galaxy luminosity functions being at too high luminosity. In the Baugh05 model, this problem is solved by introducing supernova-driven *superwinds* (see Benson et al. (2003) and Lacey et al. (2008) for details), which eject gas completely from the halo at a rate proportional to the SFR, and operate alongside the standard SN feedback. Such winds have been observed in massive galaxies, with the inferred mass ejection rates found to be comparable to the star formation rate (e.g. Heckman et al. 1990; Pettini et al. 2001). The effect of expelling gas from halos is to reduce the density of hot gas in them and increase the radiative cooling time, resulting, in particular, in less gas cooling in massive halos. In contrast, the Bower06 model solves the same problem by introducing feedback from AGN. Halos in which the cooling time of the gas exceeds the free-fall time and which also contain a sufficiently large central supermassive black hole (SMBH) are assumed to set up a steady state in which halo gas accreting onto the SMBH releases energy in the form of relativistic jets which heat the halo gas, exactly balancing the halo cooling, and preventing any gas from cooling onto the galaxy disk. The SMBH are assumed to grow by gas accretion in starbursts triggered by galaxy mergers and disk instabilities and, less commonly, by black hole/black hole mergers (as detailed in Bower et al. 2006, Malbon et al. 2007 and Fanidakis et al. 2010). In the Bower06 model, the disk instabilities appear to be critical for producing large enough SMBH at early enough times for the AGN feedback to be effective.

The assumption of a top-heavy IMF in starbursts in the Baugh05 model is a controversial one. As discussed in detail in Baugh et al. (2005), this top-heavy IMF was found to be required in order to reproduce the observed number counts and redshift distributions of the faint sub-mm galaxies. The top-heavy IMF results both in higher bolometric and far-UV luminosities for young stellar populations, and greater production of heavy elements and hence also dust, both effects being important for reproducing the properties of SMGs in the model. Furthermore, as shown by Nagashima et al. (2005a,b), the predicted chemical abundances of the X-ray emitting gas in galaxy clusters and of the stars in elliptical galaxies also agree better with observational data in a model with the top-heavy IMF in bursts, rather than one with a universal Solar neighbourhood IMF. Subsequent work using the same model has also shown that it predicts galaxy evolution in the mid-IR in good agreement with observations by *Spitzer* (Lacey et al. 2008). A more detailed comparison of the model with the properties of observed SMGs has been carried out by Swinbank et al. (2008), and an investigation of the present-day descendants of SMGs in Gonzalez et al. (2010b). As shown by Le Delliou et al. (2006) and Orsi et al. (2008), the same model also reproduces the observed evolution of the luminosity function and clustering of Lyα-emitting galaxies at high redshift.

A variety of other observational evidence has accumulated which suggests that the IMF in some environments may be top-heavy compared to the Solar neighbourhood IMF (see Elmegreen 2009 for a recent review). Rieke et al. (1993) argued for a top-heavy IMF in the nearby starburst M82, based on modelling its integrated properties, while Parra et al. (2007) found possible evidence for a top-heavy IMF in the ultra-luminous starburst Arp220 from the relative numbers of supernovae of different types observed at radio wavelengths. Evidence has been found for a top-heavy IMF in some star clusters in intensely star-forming regions, both in M82 (e.g. McCrady et al. 2003), and in our own Galaxy (e.g. Figer et al. 1999; Stolte et al. 2005; Harayama et al. 2008). Observations of

both the old and young stellar populations in the central 1 pc of our Galaxy also favour a top-heavy IMF (Paumard et al. 2006; Maness et al. 2007). In the local Universe, Meurer et al. (2009) find evidence for variations in the IMF between galaxies from variations in the Hα/UV luminosity ratio. Fardal et al. (2007) found that reconciling measurements of the optical and IR extragalactic background with measurements of the cosmic star formation history also seemed to require an average IMF that was somewhat top-heavy. Pérez-González et al. (2008) compared observational constraints on the evolution of the star formation rate density and stellar mass density over cosmic time, and found that reconciling these two types of data also favours a more top-heavy IMF at higher redshifts, as had been hinted at by earlier studies. Finally, van Dokkum (2008) found that reconciling the colour and luminosity evolution of early-type galaxies in clusters also favoured a top-heavy IMF. Larson (1998) summarized other evidence for a top-heavy IMF during the earlier phases of galaxy evolution, and argued that this could be a natural consequence of the temperature dependence of the Jeans mass for gravitational instability in gas clouds. Larson (2005) extended this to argue that a top-heavy IMF might also be expected in starburst regions, where there is strong heating of the dust by the young stars.

2.2 Dust extinction.

The attenuation of starlight by dust is a crucial part of our model, since LBGs are detected by their rest-frame far-UV emission, which appears to be heavily extincted. In our earlier investigation of LBGs in Baugh et al. (2005), we calculated both the absorption and emission of starlight by dust in model galaxies by coupling `GALFORM` to the `GRASIL` spectrophotometric code (Silva et al. 1998), which incorporates a radiative transfer calculation of starlight through a realistic dust distribution, and a detailed model of heating and cooling of dust grains (including PAH molecules). The `GRASIL` model assumes a composite disk plus spheroid geometry for quiescent galaxies, with stars in both components, but dust only in the disk. In the case of ongoing bursts, this is replaced by a stellar spheroid plus a flattened burst component containing the dust, and having the same half-mass radius as the spheroid. The dust is assumed to be in two phases, a diffuse medium and also giant molecular clouds in which the stars form, and from which they escape after a few Myr. The coupled `GALFORM`+`GRASIL` model is described in Granato et al. (2000).

The `GRASIL` model is computationally expensive, since it involves a detailed radiative transfer calculation for each model galaxy, and furthermore in the present paper we only need to calculate the extinction of starlight from galaxies, and not the IR/sub-mm dust emission. In this paper, we therefore calculate dust extinction using an alternative approach, which assumes the same geometry for the stars and dust as in `GRASIL`, but gains in computational speed by making some simplifying approximations. This alternative method is described in detail in Lacey et al. (2010a), where we also show that it gives very similar results to `GRASIL` for the dust extinction and for the far-IR (but not mid-IR) emission from dust. Here we give a brief summary of how dust extinction is calculated in this alternative approach.

The starting point of the approach used here is the model for extinction by diffuse, smoothly distributed dust described in Cole et al. (2000), to which we add a treament of extinction of young stars by molecular clouds. We calculate the extinction by the diffuse component of the dust using the tabulated radiative transfer models of Ferrara et al. (1999), which assume that the stars

are in both a disk and a spheroid, and that the dust is uniformly mixed with the stars in the exponential disk, with a Milky Way extinction law. This already gives very different extinctions from a foreground screen model with the same column density of dust. The Ferrara et al. models give dust attenuation factors separately for the disk and spheroid light, as functions of wavelength, galaxy inclination, central face-on V-band dust optical depth, and ratio of spheroid to disk scalelengths.

The radii of the disk and spheroid of each model galaxy are predicted directly by GALFORM, as described in Cole et al. (2000), based on conservation of angular momentum (for the disk) and energy (for the spheroid), and taking account of their own self-gravity and that of the dark halo. The Ferrara et al. models assume a fixed ratio of vertical to radial exponential scalelengths for the disk stars of 0.1. We assume that the dust has the same radial and vertical scalelengths as the stars. The total mass of dust in each galaxy is calculated from the cold gas mass and metallicity predicted by GALFORM, assuming that the dust-to-gas ratio is proportional to the gas metallicity, and normalized to match the solar neighbourhood dust-to-gas ratio for solar metallicity ($Z_\odot = 0.02$). The only change relative to Cole et al. (2000) is that we assume that a fraction $f_{\rm cloud}$ of the cold gas and dust are in molecular clouds, so the mass of dust in the diffuse phase is a fraction $1 - f_{\rm cloud}$ of the total dust mass. We then calculate the central face-on optical depth of the diffuse dust from its mass and radial scalelength. Finally, we choose a random inclination angle for each model galaxy. GALFORM calculates separate disk and spheroid luminosities at each wavelength, so we interpolate in the tables and then apply the separate dust attenuation factors for the disk and spheroid light.

We model extinction by molecular clouds based on the same physical picture as in GRASIL, but by a more approximate technique. We assume that a fraction $f_{\rm cloud}$ of the cold gas and dust is in molecular clouds of mass $M_{\rm cloud}$ and radius $r_{\rm cloud}$. All stars are assumed to form inside clouds, and then to escape on a timescale $t_{\rm esc}$, such that the fraction inside clouds drops continuously from 1 for ages $\tau < t_{\rm esc}$, to 0 for $\tau > 2t_{\rm esc}$. The fraction of light produced by stars inside clouds depends on the wavelength, the past star formation and chemical enrichment history, and the IMF. This fraction is much larger at shorter wavelengths (for example, the far-UV), for which the light is dominated by massive stars with short lifetimes. Since it is only for these stars that the extinction by clouds is significant, we can approximate the recent SFR history when estimating this fraction. We assume the recent SFR to be constant in time for the case of a quiescent disk, while for an ongoing burst we use the actual exponential SFR history of that burst. The fraction of stars which are inside clouds are extincted both by the clouds and by the diffuse medium, while the remaining stars are extincted only by the diffuse medium. The extinction of stars inside clouds depends on the surface density of the clouds and on the gas metallicity, with the stars treated as being at the centre of each cloud. We then calculate the total dust attenuation by combining the attenuation factors for the diffuse dust and molecular clouds. For more details see Lacey et al. (2010a). Important features of our method are that the dust extinction varies self-consistently with other galaxy properties such as size, gas mass, and metallicity, and that young stars suffer more extinction than old stars, even at the same wavelength.

Our new extinction model thus depends on the parameters $f_{\rm cloud}$, $M_{\rm cloud}$, $r_{\rm cloud}$ and $t_{\rm esc}$. In fact, the dependence on $M_{\rm cloud}$ and $r_{\rm cloud}$ is only through the combination $M_{\rm cloud}/r_{\rm cloud}^2$ which determines the surface density of a single cloud. Our default values for these parameters are the same as we used in our GRASIL modelling in Baugh et al. (2005), namely $f_{\rm cloud} = 0.25$, $M_{\rm cloud} =$

$10^6 M_\odot$, $r_{\rm cloud} = 16{\rm pc}$ and $t_{\rm esc} = 1{\rm Myr}$. The value $t_{\rm esc}$ was adjusted in that paper to match the far-UV LF of LBGs at $z \sim 3$, while the values of the other three dust parameters were chosen in Granato et al. (2000) by comparison with observations of local galaxies. With these parameters, the extinction optical depth at 1500Å for stars at the centre of a cloud is around 90 for solar metallicity, so the far-UV light from such stars is almost completely extincted. The net attenuation by clouds will therefore be insensitive to the exact values of $M_{\rm cloud}$ and $r_{\rm cloud}$. We investigate the effects of variations in $f_{\rm cloud}$ and $t_{\rm esc}$ in §3.2.3.

2.3 Photoionization feedback.

The reionization of the intergalactic medium (IGM) by a photoionizing background suppresses the amount of gas cooling in small halos in two ways: the resulting IGM pressure inhibits collapse of gas into halos, and the radiative cooling time for gas inside halos is increased by the photoionizing background. These effects were modelled in detail by Benson et al. (2002), and found to be reasonably well approximated by a simple model in which gas cooling is completely suppressed in halos with circular velocities $V_c < V_{\rm crit}$ at redshifts $z < z_{\rm reion}$. The original Baugh05 and Bower06 models assumed $z_{\rm reion} = 6$ and $V_{\rm crit} = 60{\rm km\,s}^{-1}$ or $50{\rm km\,s}^{-1}$ respectively. This value for the reionization redshift was motivated by measurements of Gunn-Peterson absorption in quasar spectra, which imply that reionization is essentially complete by $z \approx 6$ (Fan et al. 2000; Becker et al. 2001). The values of the threshold halo circular velocity, $V_{\rm crit}$, were motivated by the numerical simulations of Gnedin (2000). Since then, measurements of the Thomson scattering optical depth from fluctuations in the cosmic microwave background have converged to imply a higher reionization redshift, $z \sim 10 - 12$ (Dunkley et al. 2009). We therefore adopt a standard value $z_{\rm reion} = 10$ in the current sudy. More recent numerical simulations of the effect of reionization on collapse and cooling of gas in low mass halos imply weaker photoionization feedback effects than found by Gnedin (Hoeft et al. 2006; Okamoto et al. 2008). In line with these simulations, we adopt $V_{\rm crit} = 30{\rm km\,s}^{-1}$ as our standard choice in the present work. For brevity, we will refer to the slightly modified Baugh05 and Bower06 models with $z_{\rm reion} = 10$ and $V_{\rm crit} = 30{\rm km\,s}^{-1}$ simply as Baugh05 and Bower06 in what follows. We have not changed any other model parameters from their original values.

2.4 Halo merger trees

GALFORM calculates the evolution of galaxies in halo merger trees which describe the assembly and merger histories of dark matter halos. The halo merger trees are either computed using a Monte Carlo method based on the extended Press-Schechter model (Cole et al. 2000), or extracted from N-body simulations of the dark matter (Helly et al. 2003). The Baugh et al. (2005) results were based on Monte Carlo trees, while those of Bower et al. (2006) were based on N-body trees extracted from the Millennium simulation (Springel et al. 2005). Cole et al. (2008) found some differences between the Monte Carlo and N-body trees, as a result of which Parkinson et al. (2008) developed a modified version of the Cole et al. (2000) Monte Carlo algorithm, which brought the Monte Carlo trees into much better agreement with the N-body trees from the Millennium simulation. In this paper, we run both the Baugh05 and Bower06 models on Monte Carlo trees generated using the Parkinson et al. (2008) method. This has the advantage that

we can resolve much smaller halos at high redshifts than is possible using the Millennium simulation, which only resolves halos larger than $2 \times 10^{10} h^{-1} M_{\odot}$. In contrast, for the Monte Carlo trees used here, we resolve progenitor halos larger than $8 \times 10^{7} h^{-1} M_{\odot}$ for model galaxies output at $z = 3$, $1.5 \times 10^{7} h^{-1} M_{\odot}$ at $z = 6$, and $4 \times 10^{6} h^{-1} M_{\odot}$ at $z = 10$. This higher mass resolution is important for predictions of LBGs at higher redshifts and lower luminosities. The change to Parkinson et al. Monte Carlo trees leaves the predictions published in Baugh et al. (2005) and Bower et al. (2006) unchanged.

3   EVOLUTION OF LBG LUMINOSITY FUNCTION

In this section, we show the predictions of the models for the evolution of the rest-frame far-UV luminosity function (LF), and compare these with observational data for LBGs. The far-UV LF is one of the most basic observable properties of LBGs, since they are detected via their rest-frame far-UV emission, and is also of fundamental importance, since the rest-frame far-UV emission is closely related to the SFR. For the purpose of this paper, we will define model LBGs to include all galaxies with far-UV (1500Å) luminosities in the relevant range, regardless of whether they satisfy the observational colour-selection criteria used in specific surveys, as discussed futher below.

3.1   Comparison of Baugh05 and Bower06 models

We start by showing in Fig. 1 the evolution of the dust-extincted rest-frame 1500Å LFs over a large range in redshift and luminosity, for both the Baugh05 and Bower06 models (top and bottom panels respectively). For clarity, we show the evolution separately for $3 < z < 7$ (left panels) and $7 < z < 20$ (right panels). The solid lines show the total LF, while the dashed lines show the contribution to the LF from ongoing bursts. There are a number of interesting features in these plots. Both models show relatively mild evolution in the far-UV LF in the redshift range $3 \lesssim z \lesssim 8$, with a gradual decrease in comoving number density with increasing redshift at most luminosities, followed by a much steeper decline in number density at $z \gtrsim 8$. This rapid evolution at high redshifts is driven by the build-up of the dark matter halos hosting the LBGs, and was also found ealier in GALFORM predictions for the LFs of Lyα-emitting galaxies (LAEs), which are a population closely related to the LBGs (Le Delliou et al. 2006). However, the LFs in the two models have distinctly different shapes.

In the Baugh05 model, the LF has a steep, quasi-exponential, cutoff at high luminosities, with a flattening or bump at lower luminosities, followed by an upturn and steeper power-law slope at the faintest luminosities. This behaviour is due to the major role played by merger-driven starbursts in the Baugh05 model. As can be seen from the dashed lines in the figure, starbursts dominate the bright end of the LBG LF, while quiescent galaxies (with star formation occuring in the disk) dominate the faint end. The LF of the starbursts actually declines at low luminosities, which is what causes the bump seen in the LF. The steep faint end is due to the quiescent population. In the Bower06 model, on the other hand, the LFs show a more power-law behaviour over the ranges plotted here, with a gradual steepening from low to high luminosity. There is a sharper break at the highest luminosities, but this is at much higher luminosities and lower number densities than in the Baugh05 model. These differences are due to various effects. In the Bower06 model, ongoing starbursts do not dominate the LBG LF at any luminosity

once dust extinction is included. However, due to the much shorter burst timescales in the Bower06 model, there is an important contribution to the far-UV LF from bursts which have recently terminated. In such cases, star formation has ceased, and the gas and dust associated with the burst have already been consumed or dispersed, but many of the massive stars produced during the burst are still shining in the far-UV. Such recently terminated bursts in fact dominate the bright end of the far-UV LF in the Bower06 model over the whole range of redshifts plotted in Fig. 1, and are responsible for the larger number of objects seen at the highest luminosities compared to the Baugh05 model. The dust extinction in these objects is low, as discussed further below. The shallower slope seen at the faintest luminosities in the Bower06 model is due to the stronger SN feedback. Even the LF for ongoing starbursts has a flatter shape in the Bower06 model, because bursts are triggered mainly by disk instabilities rather than galaxy mergers.

We next compare the predicted far-UV LFs from the models with observational estimates of the LFs derived from samples of LBGs at redshifts $z = 3 - 10$. The observational selection is typically based on two colours, one of which straddles the Lyman break at the target redshift, and the other which measures the spectral slope longwards of the break, and is used to exclude contaminants, principally lower redshift galaxies and galactic stars, which have redder colours than expected for a star forming galaxy at the target redshift. The observational LFs we plot already include corrections by the original authors for the completeness as a function of redshift and luminosity, as well as for absorption by the IGM (where appropriate), but do not include corrections for dust extinction. We therefore compare our model LFs, including dust extinction, directly with the LFs inferred observationally. Each LBG survey uses its own set of filters, so in practice they measure the far-UV LFs at slighly different effective rest-frame wavelengths, in the range 1350–1700Å. We plot our model LFs at a fixed rest-frame wavelength of 1500Å, so, in principle, we should correct the luminosities for this small wavelength difference when comparing with the observational data. However, the spectra of LBGs are observed to be fairly flat in this wavelength range, so this correction is small, and we neglect it here. It is also possible that the observed luminosity functions are effectively missing some galaxies due to the colour selection, even after the completeness corrections applied by the original authors (e.g. due to the galaxies being too red in the far-UV due to dust extinction). Different completeness corrections have been applied in different surveys, and this presumably accounts for some of the differences seen in the inferred LFs. In contrast, our model LFs include all galaxies at a given 1500Å luminosity, regardless of their far-UV colour. We defer to a future paper a detailed study of the effect of applying different LBG colour selections directly to the models, and the effect this has on the completeness of the galaxy samples at far-UV wavelengths. The observational LFs are all plotted for the same cosmology ($\Omega_m = 0.3$, $\Omega_\Lambda = 0.7$) as used in the Baugh05 model (correcting to this cosmology if needed). The cosmology used in the Bower06 model is slightly different, but converting the observational data to it would have little effect on the comparison, so we ignore this correction here.

We compare the 1500Å LFs from the Baugh05 and Bower06 models with the observed far-UV LFs in Figs. 2 and 3. Fig. 2 shows redshifts $z = 3, 4, 5, 6$ and Fig. 3 shows $z = 7, 8, 10$. The Baugh05 model is shown in blue, and the Bower06 model in magenta. In both cases, we plot the dust-extincted LF as a solid line, and the unextincted LF as a dashed line. The Baugh05 model fits the observational data well over the whole redshift range $z = 3 - 10$,
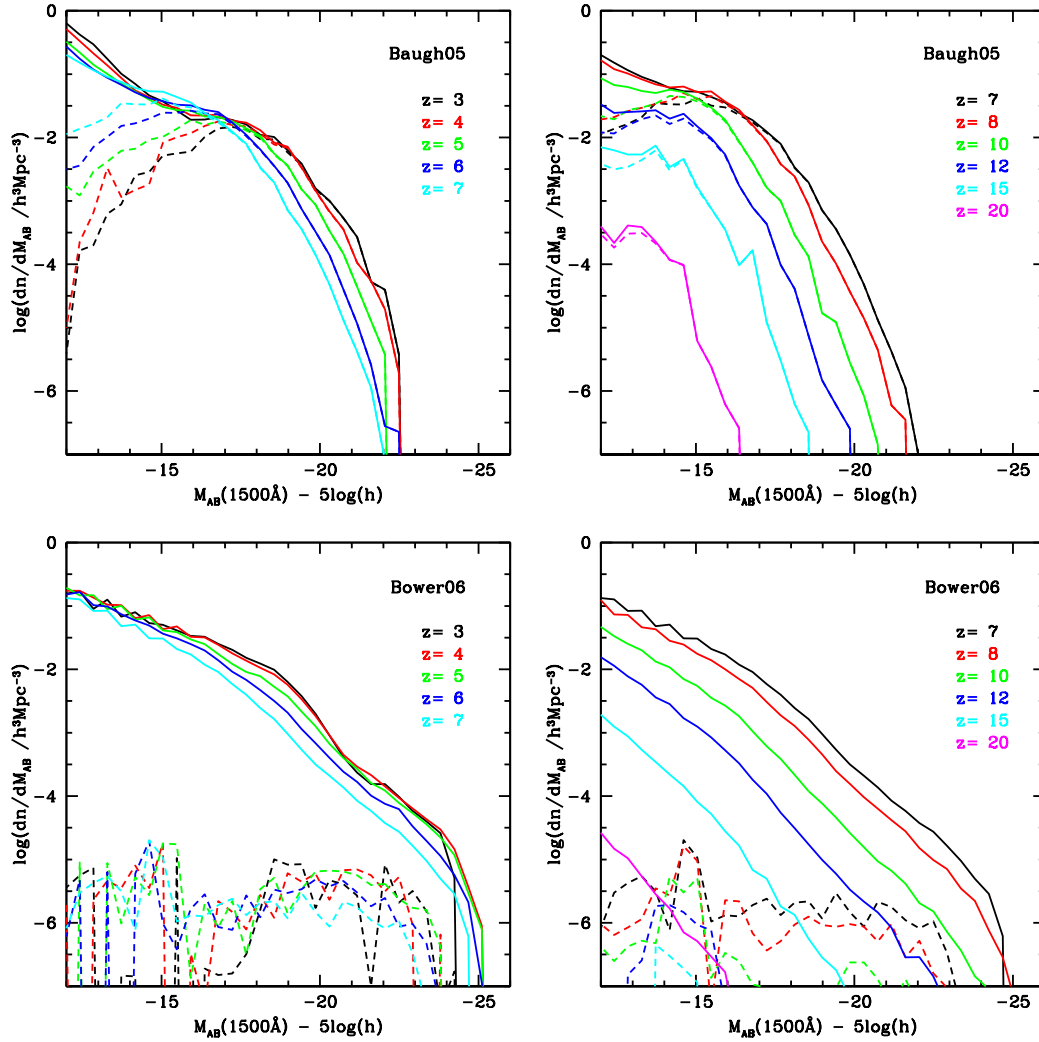
Figure 1. Predicted evolution of the rest-frame far-UV (1500Å) luminosity function of LBGs in the Baugh05 model (top panels) and the Bower06 model (bottom panels). In both cases, the left panels show the evolution for $3 < z < 7$ and the right panels for $7 < z < 20$, with different redshifts shown in different colours, as indicated by the key. The dashed lines show the contribution from ongoing starbursts. All of the LFs plotted here include dust extinction.

when we include dust extinction. This is remarkable when we consider that we have not changed any model parameters from those published in Baugh et al. (2005), apart from $z_{\rm reion}$ and $V_{\rm crit}$ (as described in §2), whose effect is anyway quite small. We used the observed far-UV LBG LF at $z = 3$ to constrain the model parameters in Baugh et al. (2005), but we did not use observations of LBGs at any other redshift. In contrast, the Bower06 model is in much worse agreement with the observed LBG LFs at almost all of the redshifts plotted, predicting far more very luminous galaxies than observed. The Bower06 model in its original form can therefore be excluded based on this observational data.

By comparing the solid and dashed lines, we can assess the effect of dust extinction on the predicted LFs. For the Baugh05 model, the effect of dust extinction is very large over the luminosity range covered by the observational data, causing the LF to be shifted faintwards by $\sim 1.5 - 2.5$ mag at the bright end. In contrast, the effects of dust extinction are generally smaller in the Bower06 model, especially at the highest luminosities. An important factor in this is that the gas metallicity of the LBGs is typically much larger in the Baugh05 than Bower06 model, leading

to higher dust-to-gas ratios. The higher metallicities, in turn, result from the top-heavy IMF assumed for starbursts in the Baugh05 model, which leads to a higher yield of heavy elements from Type II supernovae. However, another important factor is the much shorter timescale for bursts in the Bower06 model (~ 0.001 Gyr or less as against $\sim 0.01 - 0.1$ Gyr in the Baugh05 model). A consequence of this is that the bright end of the far-UV LF in the Bower06 model is dominated by bursts which have terminated within the last $\sim 0.01 - 0.1$ Gyr. For these objects, most of the massive stars formed during the burst are still shining, but the dust which shrouded the burst while it was ongoing has gone. As a result, they have large far-UV luminosities but very little dust extinction.

Using a different semi-analytical model, Lo Faro et al. (2009) predicted a significant excess of faint LBGs compared to observational data at $z \sim 4 - 5$. We do not see such an excess in our own model, even though we compare to similar observational data. This is most likely due to the different treatments of supernova and photoionization feedback in the Lo Faro et al. model. The effects of varying the treatment of supernova and photoionization feedback in our own model are discussed below in §3.2.1 and §3.2.5.
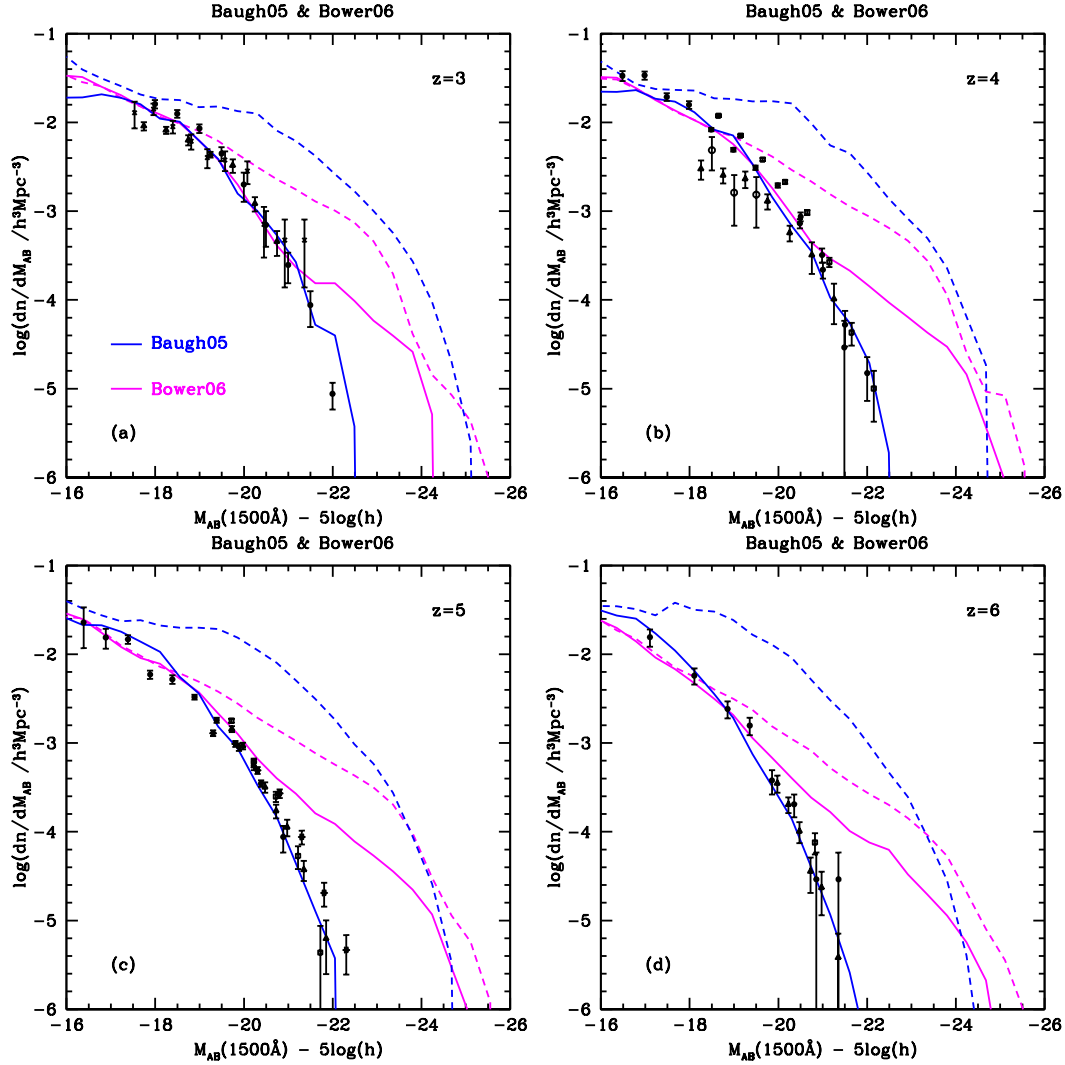
Figure 2. Predicted rest-frame 1500Å LFs for the Baugh05 model (blue) and Bower06 model (magenta) compared to observational data from LBG surveys. Solid and dashed lines show LFs with and without dust extinction. (a) $z = 3$. (b) $z = 4$. (c) $z = 5$. (d) $z = 6$. The observational data are as follows (with rest-frame wavelength): $z = 3$ – Arnouts et al. (2005) (crosses, 1500Å), Sawicki & Thompson (2006) (empty triangles, 1700Å), Reddy & Steidel (2009) (filled circles, 1700Å); $z = 4$ – Steidel et al. (1999) (empty circles, 1700Å), Sawicki & Thompson (2006) (empty triangles, 1700Å), Yoshida et al. (2006) (empty squares, 1500Å), Bouwens et al. (2007) (filled circles, 1600Å); $z = 5$ – Yoshida et al. (2006) (empty squares, 1500Å), Iwata et al. (2007) (stars, 1600Å), Bouwens et al. (2007) (filled circles, 1600Å), McLure et al. (2009) (empty triangles, 1500Å); $z = 6$ – Shimasaku et al. (2005) (open squares, 1400Å), Bouwens et al. (2007) (filled circles, 1350Å), McLure et al. (2009) (empty triangles, 1500Å).

3.2 Effects of varying model parameters

We now consider the effects on the far-UV LFs of varying some of the key parameters in GALFORM. Since the default Baugh05 model has been shown to agree much better with the observed LBG LFs than the default Bower06 model, we consider here only parameter variations around the default Baugh05 model. Our purpose here is to understand the sensitivity of the LBG predictions to different parameters. We emphasize that most of the parameter variations we consider do not lead to models that we would consider acceptable overall, since we require our model to fit a much wider range of observational data than just LBGs, as discussed in §2.

3.2.1 Photoionization feedback

Photoionization feedback is described by the parameters z_{reion} and V_{crit}. In Fig. 4, we compare the far-UV LFs for our default values of these parameters ($z_{\mathrm{reion}} = 10$, $V_{\mathrm{crit}} = 30\mathrm{km\,s^{-1}}$, blue curves) with the values used in the original Baugh et al. (2005) paper ($z_{\mathrm{reion}} = 6$, $V_{\mathrm{crit}} = 60\mathrm{km\,s^{-1}}$, green curves), and with the case $z_{\mathrm{reion}} = 10$, $V_{\mathrm{crit}} = 60\mathrm{km\,s^{-1}}$ (red curves). We only show this comparison at $z = 3$ and $z = 6$; for $z \geqslant 10$ the three models are identical. At $z = 6$, the model with $z_{\mathrm{reion}} = 6$ and $V_{\mathrm{crit}} = 60\mathrm{km\,s^{-1}}$ is slightly above the default model at the faint end of the LF. This is because photoionization feedback has only just turned on in the former model, and so has not had time to have any effect on galaxy luminosities. On the other hand, by $z = 3$, the model with $z_{\mathrm{reion}} = 6$ and $V_{\mathrm{crit}} = 60\mathrm{km\,s^{-1}}$ is somewhat below the default model at the faint end. This is be-
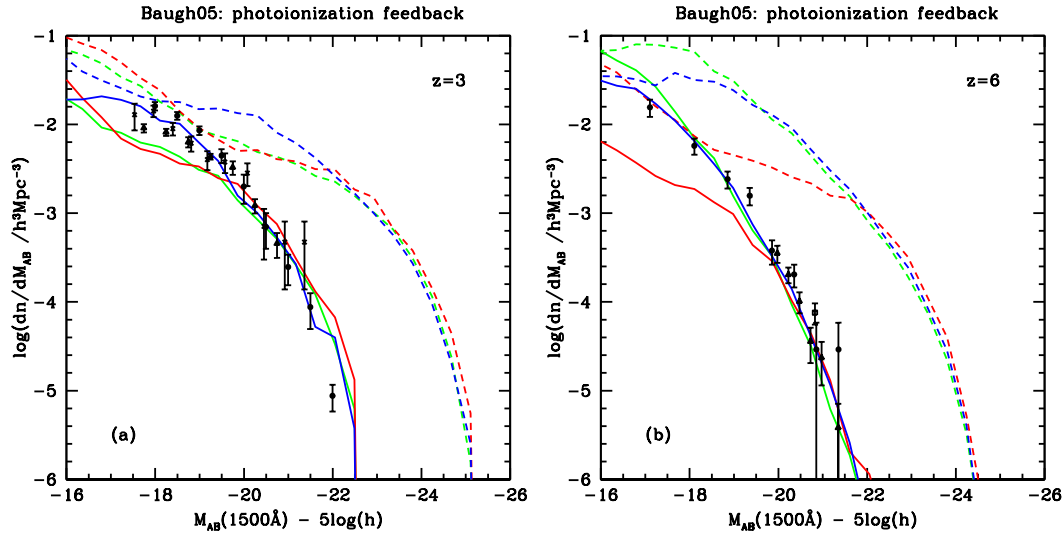
Figure 4. Predicted rest-frame 1500Å LFs for the Baugh05 model, showing the effect of varying the photoionization feedback parameters, at (a) $z = 3$ and (b) $z = 6$. The blue lines show the default model ($z_{\rm reion} = 10$, $V_{\rm crit} = 30{\rm km\,s}^{-1}$), green lines show the case where $z_{\rm reion} = 6$, $V_{\rm crit} = 60{\rm km\,s}^{-1}$, and red lines show the case $z_{\rm reion} = 10$, $V_{\rm crit} = 60{\rm km\,s}^{-1}$. The solid and dashed lines show the LFs with and without dust extinction, as before, and the observational data are the same as plotted in Fig. 2.

cause the effect of photoionization feedback is much stronger with $V_{\rm crit} = 60{\rm km\,s}^{-1}$ than $V_{\rm crit} = 30{\rm km\,s}^{-1}$ (the halo mass affected scales approximately as $V_{\rm crit}^3/(1 + z)^{3/2}$). The model with $z_{\rm reion} = 10$ and $V_{\rm crit} = 60{\rm km\,s}^{-1}$ shows a large suppression of the faint end of the LF at $z = 6$ relative to the default model, but by $z = 3$ the predicted LF is very similar to that for $z_{\rm reion} = 6$ and $V_{\rm crit} = 60{\rm km\,s}^{-1}$. This shows that the predicted LF becomes insensitive to the value of $z_{\rm reion}$ at much later epochs. The reduction in $V_{\rm crit}$ for the present default model relative to Baugh et al. (2005) also causes a slight steepening in the present-day galaxy luminosity function, but only for galaxies fainter than $M_B - 5 \log h \sim -16$. For the Bower06 model, the change in $V_{\rm crit}$ and $z_{\rm reion}$ from the values used in Bower et al. (2006) has negligible effects on either the LBG LFs shown here or on the $z = 0$ luminosity functions. This is because the stronger SN feedback assumed in the Bower06 model dominates over the effect of photoionization feedback in low-mass galaxies.

3.2.2 IMF and starbursts

Starbursts and a top-heavy IMF play crucial roles in the Baugh05 model, so we next consider the effects of changes in these components in Fig. 5. We show comparisons of the far-UV LFs for $z = 3, 6, 10$ to span the range of current observational data on LBGs. In these panels, the blue line shows the default model with starbursts triggered by all major galaxy mergers and some minor mergers, with a top-heavy IMF in all of these starbursts. We emphasize that, according to the results of Baugh et al. (2005), all of these ingredients are required in order that the model reproduce the number counts and redshift distributions of sub-mm galaxies. The magenta line shows the effect of turning off starbursts completely. In this case, the predicted LFs are far below the observations. This is because, in the Baugh05 model, we deliberately chose a star formation timescale in quiescent disks which is long compared to the Hubble time at high redshift, so that disks at high redshift are gas-rich, providing more fuel for star formation in starbursts. As a less extreme variation, we consider allowing bursts to be triggered by

major galaxy mergers only, shown by the green lines. In this case, the changes in the LF are smaller but still significant (factors of a few at all plotted luminosities), implying that most LBGs in the model are bursts triggered by minor mergers. Finally, we show by the red lines the effects of assuming a Kennicutt IMF in bursts (the same as for quiescent star formation), rather than a top-heavy IMF. In this case, the effects on the LF are mainly at the bright end. Compared to the default model, there is a large change in the unextincted LFs, but a smaller change after dust extinction is included. This is because the top-heavy IMF in bursts has two effects on the far-UV LF which partly cancel each other: there are more massive stars, and so higher intrinsic UV luminosities, but there is also more dust, due to increased metal production, and so more dust extinction. The relatively modest differences between the dust-extincted LBG LFs with and without the top-heavy IMF show that fitting these data does not by itself provide a strong argument for introducing variations in the IMF, although the fit is clearly better with the top-heavy burst IMF. The slope of the top-heavy IMF assumed in the Baugh05 model, $x = 0$ (§2), is quite extreme. However, the exact value of the slope is not important; any IMF with a low-mass cutoff $\gtrsim 5M_\odot$ would produce similar results.

3.2.3 Dust extinction

As already discussed, dust extinction has a large effect on the predicted LBG LF. In Fig. 6, we show the effects of varying the two key adjustable parameters in our dust model, $f_{\rm cloud}$, the fraction of the ISM in molecular clouds (which affects the attenuation by the diffuse dust), and $t_{\rm esc}$, the timescale for stars to escape from the clouds in which they are born (which affects the attenuation by molecular clouds). The blue curves show the LFs for the default values ($f_{\rm cloud} = 0.25$ and $t_{\rm esc} = 1{\rm Myr}$). The green and cyan curves show the effect of increasing $t_{\rm esc}$ to 3 Myr and 10 Myr respectively, while keeping $f_{\rm cloud}$ fixed at 0.25, while the red and magenta curves show the effect of increasing $f_{\rm cloud}$ to 0.75 and 1 respectively, while keeping $t_{\rm esc}$ fixed at 1 Myr. The dust-extincted LF is seen to be quite sensitive to increasing the escape time from
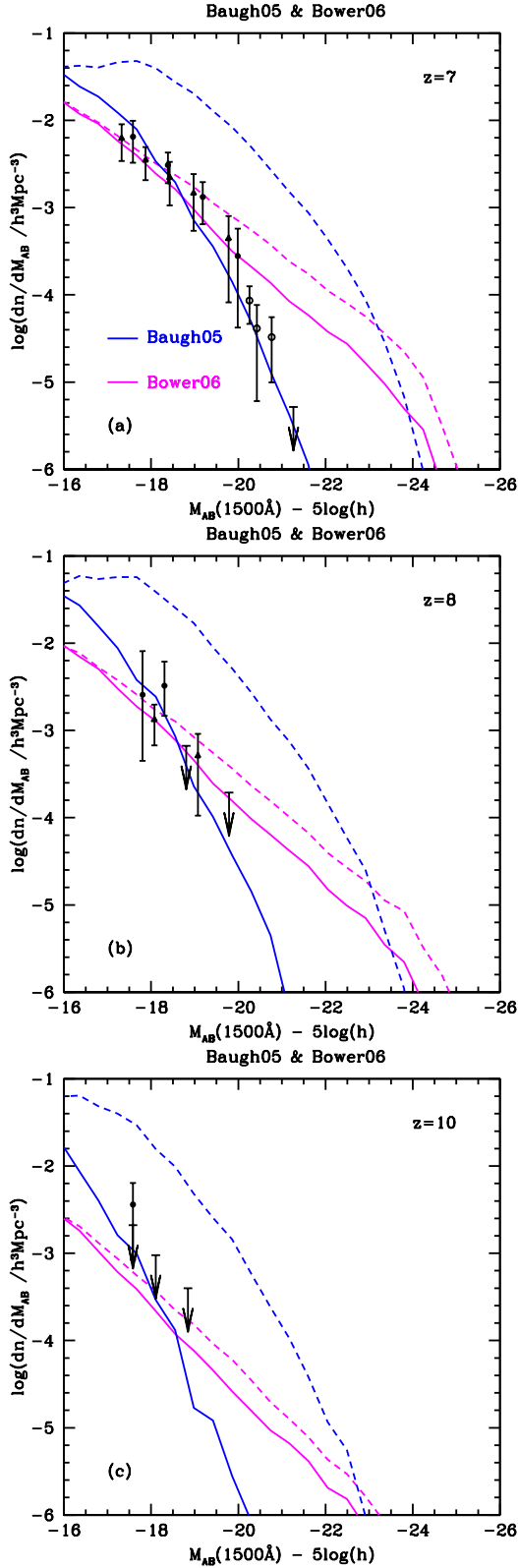
Figure 3. Predicted rest-frame 1500Å LFs for the Baugh05 model (blue) and Bower06 model (magenta) compared to observational data for LBGs. Solid and dashed lines show LFs with and without dust extinction. (a) $z = 7$. (b) $z = 8$. (c) $z = 10$. The observational data are as follows (with rest-frame wavelength): $z = 7$ – Ouchi et al. (2009) (empty circles and upper limits, 1500Å), Oesch et al. (2010b) (filled circles, 1600Å), McLure et al. (2010) (empty triangles, 1500Å); $z = 8$ – Bouwens et al. (2010) (filled circles and upper limits, 1700Å), McLure et al. (2010) (empty triangles, 1500Å); $z = 10$ – Bouwens et al. (2009b) (filled circles and upper limits, 1600Å).
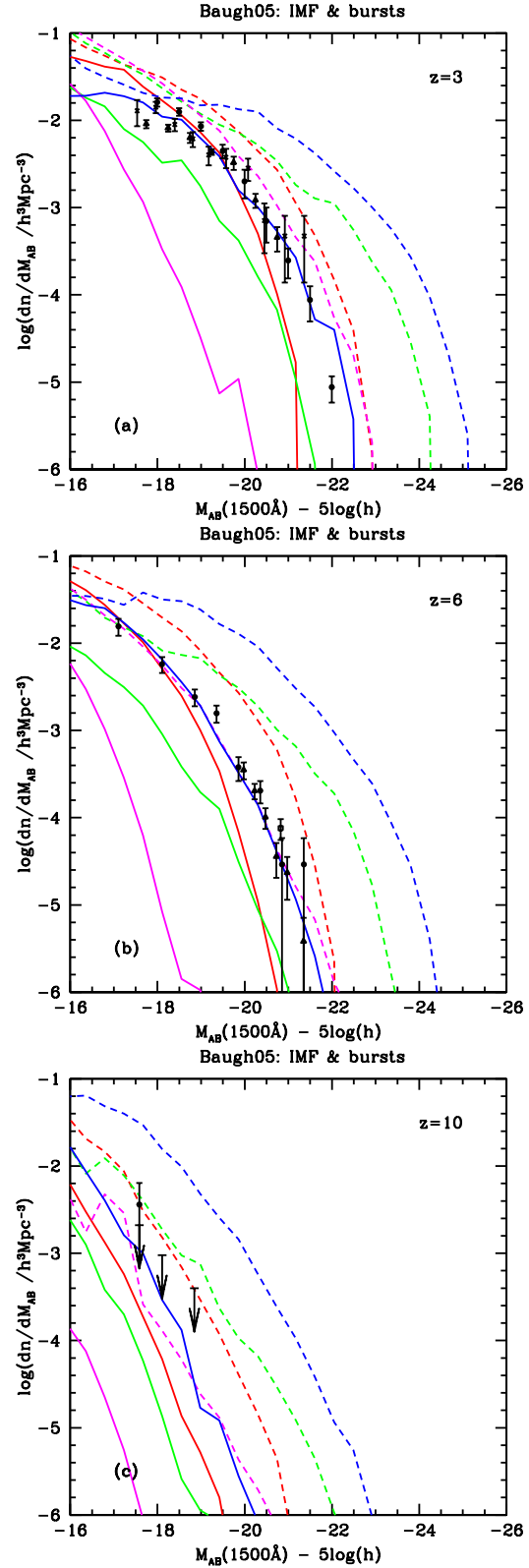
Figure 5. Predicted rest-frame 1500Å LFs for the Baugh05 model, showing the effects of varying the parameters for bursts. (a) $z = 3$. (b) $z = 6$. (c) $z = 10$. Blue lines – default model; red – Kennicutt IMF in bursts; green – bursts triggered by major mergers only; magenta – no bursts. The observational data are the same as plotted in Figs. 2 and 3.
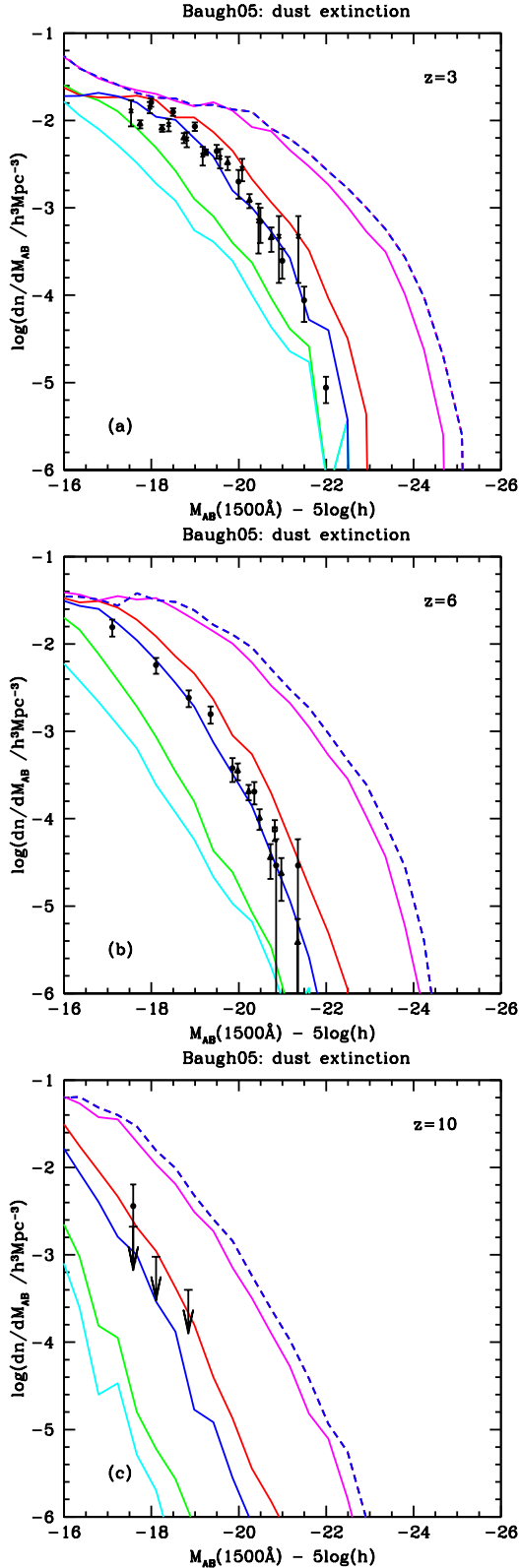
Figure 6. Predicted rest-frame 1500Å LFs for the Baugh05 model, showing the effects of varying parameters controlling dust extinction in the model. (a) $z = 3$. (b) $z = 6$. (c) $z = 10$. The dashed blue line in each panel shows the LF without dust extinction, while the solid lines show LFs with dust extinction parameters as follows: blue – default model ($t_{esc} = 1$Myr, $f_{cloud} = 0.25$); green – $t_{esc} = 3$Myr; cyan – $t_{esc} = 10$Myr; red – $f_{cloud} = 0.75$; magenta – $f_{cloud} = 1$.

its default value, reflecting the fact that a larger fraction of the UV light is absorbed within the clouds when t_{esc} is increased. This effect is especially strong in the Baugh05 model due to the top-heavy IMF assumed for bursts, which means that the UV emission is dominated by even higher mass stars than for a normal IMF. For the $x = 0$ IMF, 90% of the 1500Å light (integrated over time) is emitted by stars with lifetimes $\lesssim 10$Myr, as compared to lifetimes $\lesssim 100$Myr for the Kennicutt IMF. The LF is also seen to be insensitive to modest increases in f_{cloud} from its default value, but to become more sensitive as f_{cloud} approaches 1. This is because the optical depth of the diffuse dust is proportional to $1 - f_{cloud}$.

It can be seen that the effects of t_{esc} and f_{cloud} on the far-UV LF are to some extent degenerate, with a decrease in t_{esc} having a similar effect to an increase in f_{cloud}. In Baugh et al. (2005), we chose to try to match the far-UV LFs of LBGs by reducing t_{esc} in bursts from the value 10 Myr assumed in Granato et al. (2000) to 1 Myr, while keeping the same value of $f_{cloud} = 0.25$ as in the latter paper. We could probably obtain a similarly good fit to the observed LBG LFs with a larger value of t_{esc} combined with a larger value of f_{cloud}, but we do not pursue this here. In future, it might be possible to distinguish the effects of t_{esc} and f_{cloud} by comparing with observed SEDs of LBGs over a broader wavelength range, since the two components of the dust extinction have different dependences on wavelength.

Individual galaxies in the Baugh05 model selected by their extincted 1500Å luminosities are also predicted to have large far-UV extinctions, typically $\sim 1 - 2$ mag over the range of luminosity and redshift plotted in Figs. 2 and 3, though with a large scatter. There is a trend for the typical extinction to decrease somewhat with increasing redshift. Note that selecting galaxies by their extincted luminosities automatically biases against including the galaxies with the highest extinctions, which can cause the average extinction for such samples to differ from that of the underlying population as a whole. The values of dust extinction predicted by our model are similar to the observational estimates for LBGs by Bouwens et al. (2009a) at $z \sim 3$, but somewhat larger at $z \sim 6$. Bouwens et al. estimate extinctions from observed UV continuum slopes, assuming the same relation between UV slope and extinction as found by Meurer et al. (1999) for local UV-selected starbursts. However, the UV continuum slope is also sensitive to the age, metallicity and IMF of the stellar population, which could be different in high redshift galaxies compared to local samples. Furthermore, even many local galaxies show large deviations from the Meurer et al. relation (e.g Bell 2002; Buat et al. 2010). For these reasons, we defer a detailed comparison with observational estimates of dust extinction in LBGs to a future paper in which we directly compare predicted and observed far-UV colours in LBG samples.

3.2.4 Burst timescale and duration

Since starbursts play a very important role in the Baugh05 model, we investigate the effects on the LBG LFs of changing the burst timescale and duration. In Fig. 7 we show the effect of varying the parameters f_{dyn} and $\tau_{*burst,min}$ which control the SFR timescale in bursts. The blue lines show the default Baugh05 model, which assumes $f_{dyn} = 50$ and $\tau_{*burst,min} = 0.2$ Gyr. The green and cyan lines show the effect of reducing $\tau_{*burst,min}$ to 0.02 Gyr and 0.005 Gyr respectively, while keeping $f_{dyn} = 50$. This is seen to have only a small effect on the dust-extincted LF at $z = 3$ and $z = 6$, but to have a large effect at $z = 10$, where reducing $\tau_{*burst,min}$ results in a larger number of bright LBGs. The larger sensitivity to $\tau_{*burst,min}$ at higher redshifts is because the spheroid
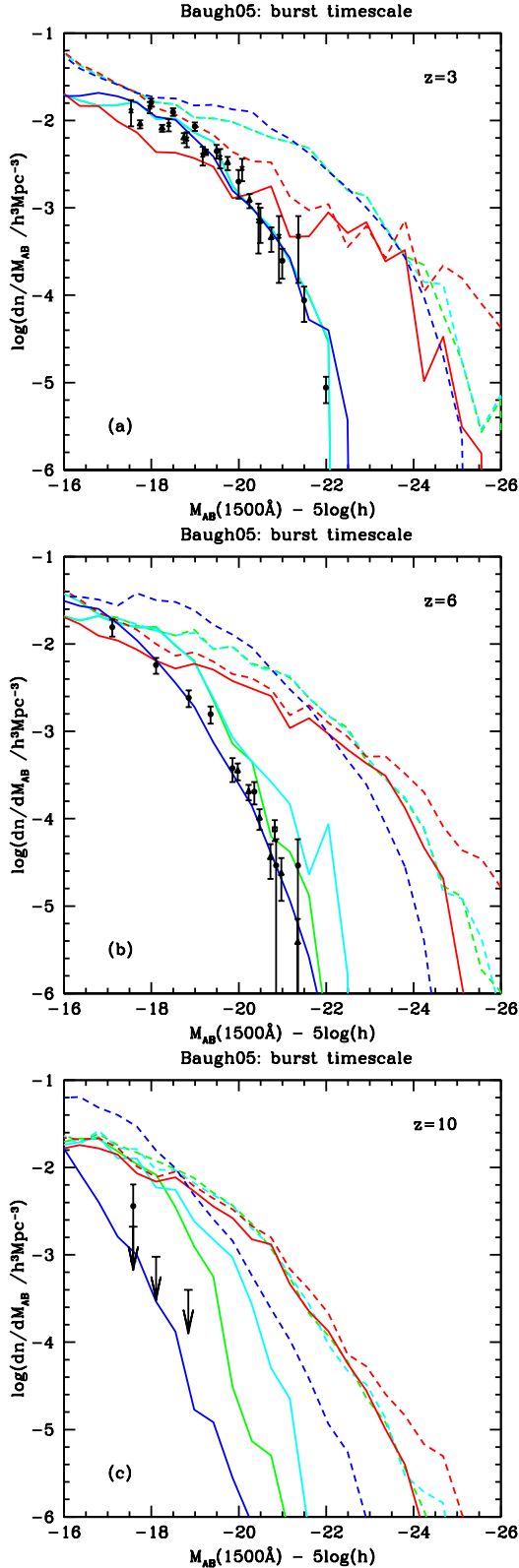
Figure 7. Predicted rest-frame 1500Å LFs for the Baugh05 model, showing the effects of varying the star formation timescale in bursts. (a) $z = 3$. (b) $z = 6$. (c) $z = 10$. Blue lines – default model ($\tau_{*\mathrm{burst,min}} = 0.2$Gyr, $f_{\mathrm{dyn}} = 50$); green – $\tau_{*\mathrm{burst,min}} = 0.02$Gyr; cyan – $\tau_{*\mathrm{burst,min}} = 0.005\ Gyr$; red – $\tau_{*\mathrm{burst,min}} = 0.005$Gyr, $f_{\mathrm{dyn}} = 2$.
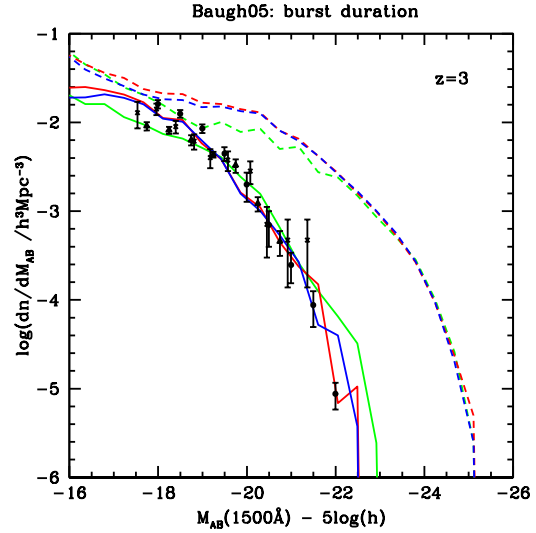
Figure 8. Predicted rest-frame 1500Å LF at $z = 3$ for the Baugh05 model, showing the effects of varying the burst duration as a multiple of its e-folding time. Blue lines – default ($n_\tau = 5$); green $– n_\tau = 1$; red $– n_\tau = 5$.

dynamical time τ_{dyn} (which enters in the burst timescale as shown in eq.(1)) is typically shorter at high-z. The red line in Fig. 7 shows the effect of reducing both f_{dyn} and $\tau_{*\mathrm{burst,min}}$ to the values $f_{\mathrm{dyn}} = 2$ and $\tau_{*\mathrm{burst,min}} = 0.005$ Gyr assumed in the Bower06 model. In this case, the effect on the dust-extincted far-UV LF is dramatic at all redshifts - there are many more very luminous LBGs and slightly fewer faint LBGs compared to the default Baugh05 model. The effects of dust extinction on the LF are also much smaller, which is the main reason for the larger number of bright galaxies in the extincted LF. The reason for the smaller dust extinction when the burst timescale is greatly reduced is that the stars that emit the 1500Å light have typical lifetimes $\sim 0.01 - 0.1$ Gyr, longer than the burst e-folding time in this case. Therefore the dust associated with the burst has mostly been consumed or ejected while these stars are still shining. This is the same effect as discussed earlier in connection with the Bower06 model. The difference in burst timescales, rather than the top-heavy IMF, seems to be the main reason why the Baugh05 model is much more successful than the Bower06 model in explaining the observed LBG LFs.

Fig. 8 shows the effect of changing the duration of bursts while keeping the star formation timescales and e-folding times fixed. The blue lines show our default model, in which the burst duration is $n_\tau = 3$ e-folding times, while the green and red curves show the effect of decreasing this to $n_\tau = 1$ or increasing it to $n_\tau = 5$. The effects are seen to be quite small, showing that the predictions for the far-UV LF are insensitive to details of the burst duration, but are more sensitive to the star formation timescale.

3.2.5 Supernova feedback

Fig. 9 shows the effect of varying the supernova feedback parameters V_{hot} and α_{hot}. We only show results for $z = 3$, since the changes for $z = 6$ and 10 are similar or smaller for the luminosity range plotted here. As before, the blue lines show the default model with $V_{\mathrm{hot}} = 300 \mathrm{km\,s}^{-1}$ and $\alpha_{\mathrm{hot}} = 2$. The green and cyan lines respectively show the effect of reducing or increasing V_{hot} by a factor 2, which causes the gas ejection rate for a given star formation rate to decrease or increase by a factor 4. We see that the LF in-
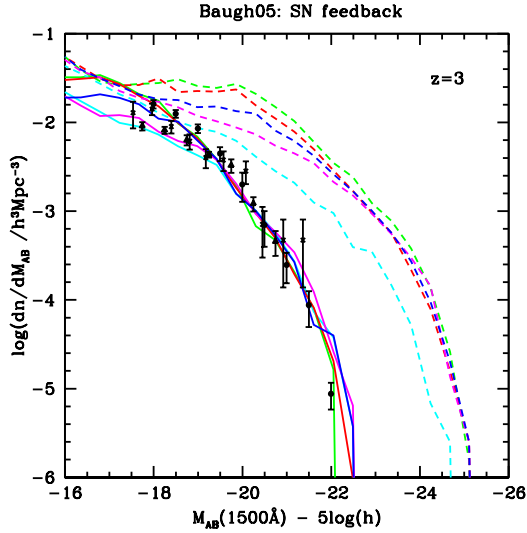
Figure 9. Predicted rest-frame 1500Å LF at $z = 3$ for the Baugh05 model, showing the effects of varying the parameters for supernova feedback. Blue lines – default; green – $V_{\rm hot} = 150 {\rm km\,s^{-1}}$; cyan – $V_{\rm hot} = 600 {\rm km\,s^{-1}}$; red – $\alpha_{\rm hot} = 1$; magenta – $\alpha_{\rm hot} = 3$.

creases or decreases at the faint end as $V_{\rm hot}$ decreases or increases. The effect is modest for the dust-extincted LF, but larger for the unextincted LF, showing that the effects of changing feedback on the stellar luminosities are to some extent compensated by changes in the dust extinction. The red and magenta lines show the effect of decreasing $\alpha_{\rm hot}$ to 1 or increasing it to 3. A larger $\alpha_{\rm hot}$ means that the feedback increases more strongly as the galaxy circular velocity decreases. Again, the galaxy LF increases or decreases at the faint end in the sense expected, though by a modest amount. We conclude that the predicted LFs in the Baugh05 model are relatively insensitive to the supernova feedback adopted, in the range covered by current observational data.

4 SIZES AND OTHER PHYSICAL PROPERTIES OF LBGS

We now present predictions for other physical properties of LBGs as functions of their rest-frame UV luminosities. For galaxy sizes, we show some results for both the Baugh05 and Bower06 models, but for the other properties, we only show the Baugh05 model, since this model is in much better agreement with observations of both LBG luminosity functions and sizes. We make a detailed comparison here with observational data on the sizes, but for reasons of space we make only brief comparisons with observational constraints on the other properties, deferring more detailed comparisons to future papers.

4.1 Sizes

Following their luminosity functions, the half-light radii of LBGs in the rest-frame far-UV are their most directly observable physical property, if HST imaging is available. GALFORM predicts sizes for the disk and bulge components of each galaxy using the method detailed in Cole et al. (2000). In summary, disk sizes are calculated assuming conservation of angular momentum of the gas that cools
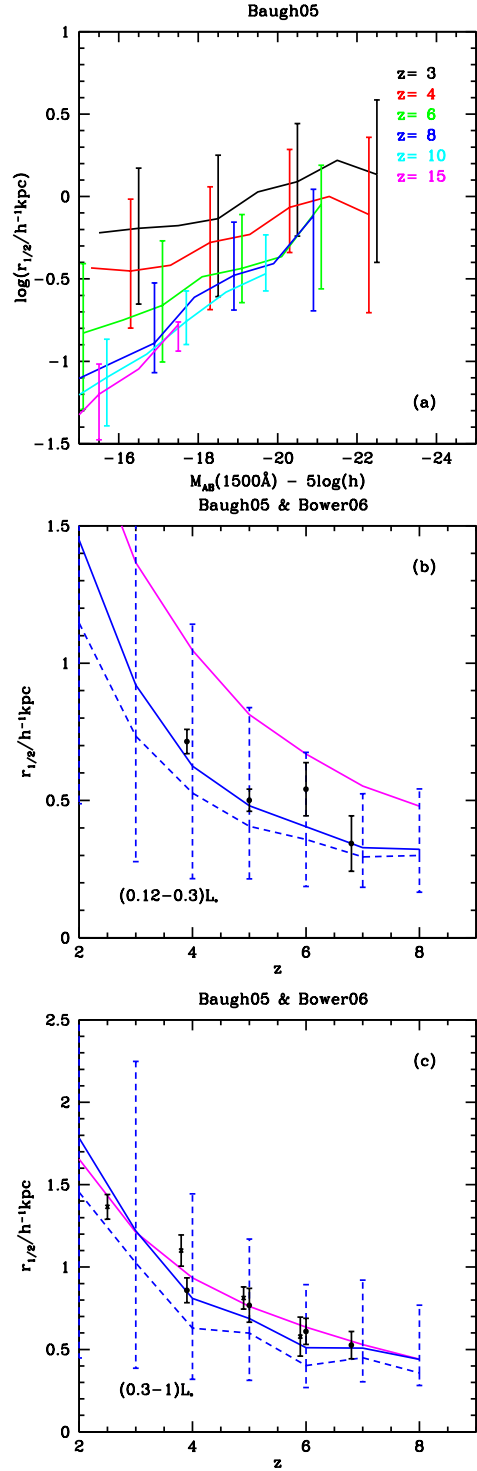
Figure 10. (a) Predicted rest-frame UV (1500Å) half-light radii of LBGs as a function of rest-frame 1500Å absolute magnitude for the Baugh05 model. Both radii and absolute magnitudes include dust extinction. The lines show median values, and the error bars show the 10-90% range. Different redshifts are shown in different colours, as indicated by the key, and have been slightly horizontally offset from each other for clarity. (b) and (c): Comparison of predicted rest-frame UV half-light radii for the Baugh05 model (blue) and Bower06 model (magenta) with observational from Oesch et al. (2010a) (filled circles) and Bouwens et al. (2004a) (crosses). Two luminosity ranges are shown, $0.12 < L(UV)/L_* < 0.3$ in (b) and $0.3 < L(UV)/L_* < 1$ in (c), equivalent to $-18.9 < M_{\rm AB}(1500{\rm Å}) - 5\log h < -17.9$ and $-20.2 < M_{\rm AB}(1500{\rm Å}) - 5\log h < -18.9$ respectively. In these two panels, the solid lines show the mean radius in that luminosity range, and the dashed lines show the medians and 10-90% percentiles (Baugh05 model only). The observational data are the mean values, with the errorbars showing the error on the mean.

out of halos, while bulge sizes are calculated assuming energy conservation when bulges form by mergers or by disk instabilities. The method allows for the gravity of the disk, bulge and dark halo, and includes the effects of halo contraction due to the gravity of the disk and bulge. Half-light radii in different bands are then calculated by combining the predicted half-mass radii and luminosities for the disk and bulge components, assuming an exponential profile for the disk and an $r^{1/4}$-law profile for the bulge.

In the top panel of Fig. 10, we show the predicted median half-light radii (at rest-frame 1500Å) as a function of rest-frame 1500Å luminosity for galaxies at different redshifts in the range $z = 3 - 15$, for the Baugh05 model. The stellar half-mass radii plotted in the same way are very similar to the half-light radii, so we do not show them here. (In principle they can differ if the disk and bulge components have different ages, metallicities or IMFs.) The galaxy sizes range from $\sim$ kpc for the brightest LBGs to ~ 100pc for the faintest and highest redshift LBGs. Both the Baugh05 and Bower06 models predict that sizes decrease with increasing redshift at a given far-UV luminosity, although by factors that depend on the model and on the galaxy luminosity. This size evolution reflects that for the host dark matter halos, for which the size scales as $M_{\rm halo}^{1/3}(1+z)^{-3/2}$ at the redshifts shown here, but it differs in detail. The ratio of galaxy to halo size is not fixed, but depends on the gas cooling and merger history (see Cole et al. 2000 for more details). The far-UV luminosity is also only indirectly related to the halo mass, depending instead on the recent star formation rate, which may correlate only weakly with halo mass, especially if bursts are important, as in the Baugh05 model.

The dependence of size on luminosity is distinctly different in the two models. In the Baugh05 model, it approaches $r \propto L^{1/3}$ at the higher redshifts plotted, but is shallower at the lower redshifts. On the other hand, the Bower06 model shows a flat or even declining dependence of size on luminosity. These dependences are similar to what the respective models predict for the dependence of disk size on luminosity in the r-band at $z = 0$, where the Baugh05 model was found to agree much better with the disk size-luminosity relation measured in the SDSS (González et al. 2009).

In the lower two panels of Fig. 10, we compare the size predictions from both models with observational data on LBGs from Bouwens et al. (2004a) and Oesch et al. (2010a), based on HST imaging in the rest-frame far-UV, and covering redshifts $2 \lesssim z \lesssim 7$. The observational data are given as mean half-light radii at different redshifts for two different far-UV luminosity ranges, specified as multiples of the observed characteristic far-UV luminosity L_* at $z = 3$ (taken by Oesch et al. to be $M_{AB}(1600\text{Å}) = -21.0$ for $h = 0.7$). We present the model predictions in the same way. The two panels show the two luminosity ranges; the solid blue and magenta lines show the mean sizes predicted by the Baugh05 and Bower06 models respectively. The blue dashed lines show the median sizes in the Baugh05 model, with the error bars indicating the 10-90% ranges. For the higher luminosity range ($0.3 < L/L_* < 1$), both models are in reasonable agreement with the observations, but in the lower luminosity range ($0.12 < L/L_* < 0.3$), only the Baugh05 model matches the observed sizes. This shortcoming of the Bower06 model results from the flat size-luminosity relation it predicts. The prediction by the Baugh05 model of LBG sizes in agreement with observations is a significant success of the model, since the only observed size information originally used in fixing the model parameters was disk sizes at $z = 0$.

We now consider a range of other physical properties for the Baugh05 model only, shown as functions of dust-extincted rest-
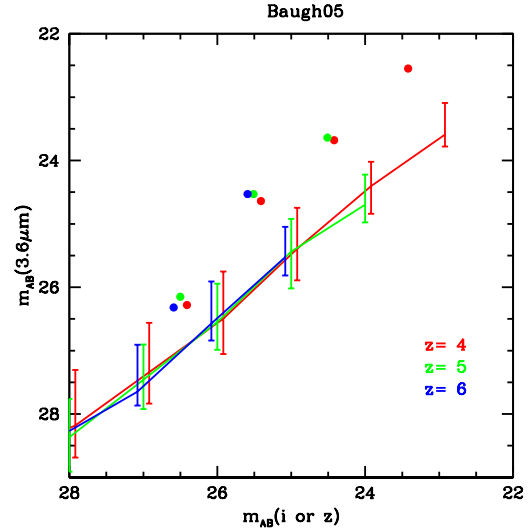

Figure 12. Relation between *Spitzer* 3.6μm and optical (i or z) apparent magnitude, for LBGs at $z = 4$ (red), $z = 5$ (green) and $z = 6$ (blue). The lines show the predicted median values in the Baugh05 model and the error bars show the 10-90% range. The filled circles show the observed median values (binned in optical magnitude) from Stark et al. (2009), for the same redshifts as the model. For clarity, small horizontal offsets have been applied to lines for different redshifts, and the same offsets have been applied to the observational datapoints.

frame far-UV luminosity for redshifts $3 < z < 15$ in Figs.11 and 13

4.2 Stellar masses

Median stellar masses are shown in the top left panel of Fig. 11. They cover a very wide range, from $\sim 10^{10}h^{-1}M_\odot$ at the highest luminosities and lowest redshifts, down to $\sim 10^5 h^{-1}M_\odot$ or less at low luminosities and high redshifts. The median stellar mass generally increases with increasing far-UV luminosity, but the dependence is flatter at lower luminosities and lower redshifts. At a given luminosity, the mass decreases with increasing redshift, but this dependence is much stronger at lower luminosities.

In general, the stars in a galaxy are a mixture of populations formed quiescently and in bursts, with different IMFs. As we discuss next, a large fraction of LBGs are predicted to be starbursts. In this case, the far-UV luminosity is generally dominated by the burst component, but the stellar mass need not be. For model LBGs at $z = 3$, $\sim 50 - 80\%$ of the stellar mass was formed quiescently in disks, and even for those LBGs which are ongoing bursts, only 10-30% of the stellar mass has formed in the current burst. At higher redshifts and lower luminosities, the fraction of the stellar mass formed in bursts increases for galaxies selected by their far-UV luminosities. For example, at $z = 6$, the fraction of stellar mass formed quiescently increases with luminosity from 20% to 80% over the range plotted here, while for the subset which are ongoing bursts, the fraction formed in the current burst decreases from $\sim 70\%$ to $\sim 10\%$ over the same range. At $z = 10$, the stellar mass in LBGs is even more dominated by burst populations, with only $\sim 10 - 30\%$ formed quiescently, and $\sim 50 - 90\%$ formed in a current burst.

The stellar masses of observed LBGs have been estimated in a number of studies, starting with $z = 3$ (Sawicki & Yee 1998;
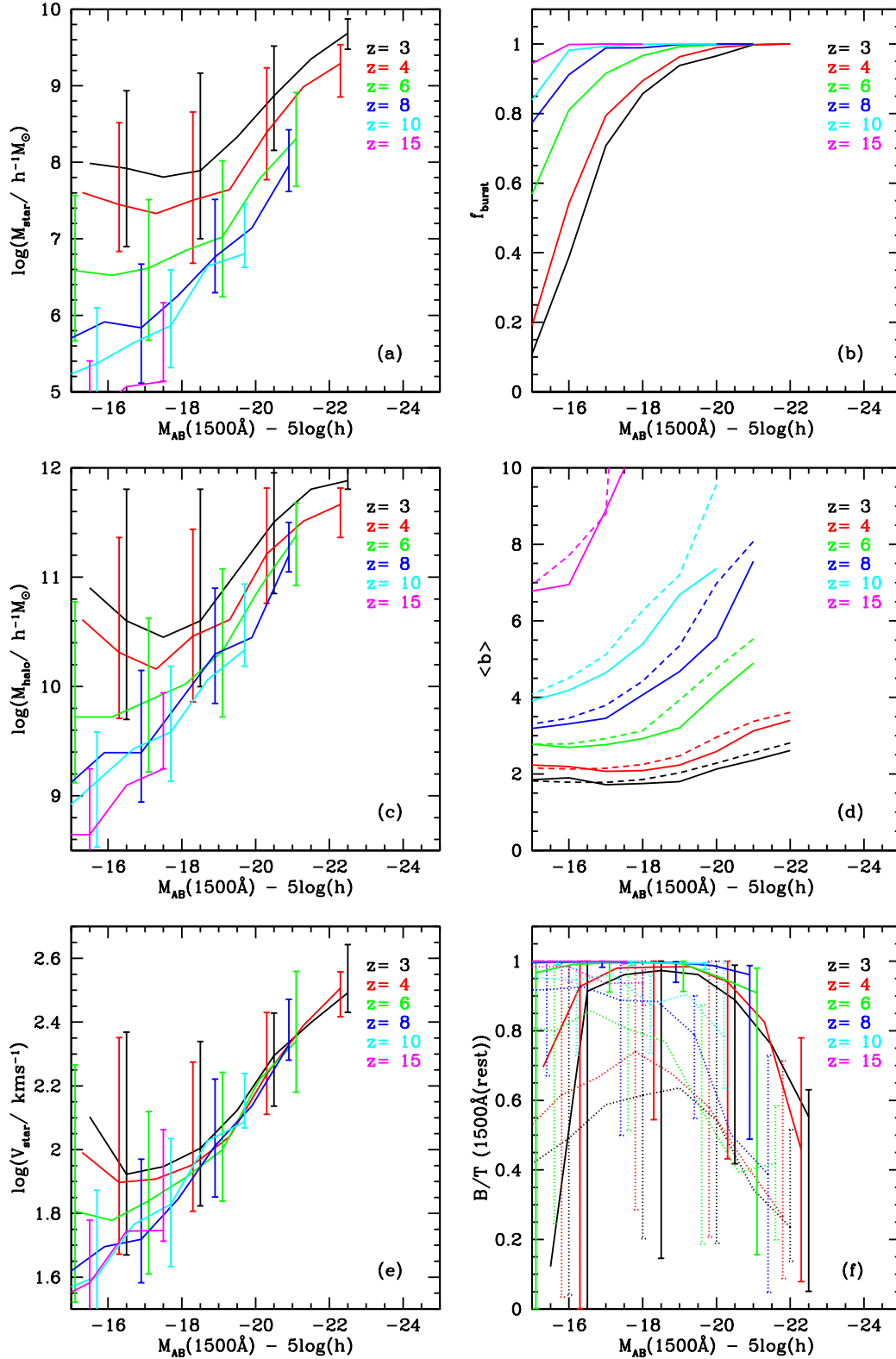
Figure 11. Predicted physical properties of LBGs as functions of dust-extincted rest-frame 1500Å absolute magnitude in the Baugh05 model. Different redshifts are shown by different colours, as indicated by the key. Unless stated otherwise, all properties are plotted as medians, with error bars showing the 10-90% range. The different panels are as follows: (a) stellar mass; (b) fraction of LBGs currently undergoing a burst; (c) dark matter halo mass; (d) mean bias (solid and dashed lines respectively show mean bias in a luminosity bin and for galaxies brighter than a given luminosity); (e) circular velocity of stars; (f) dust-extincted bulge-to-total luminosity ratio at 1500Å (with bulge-to-total stellar mass ratio shown by dotted lines).

Papovich et al. 2001; Shapley et al. 2001), and later extending to $z = 4 - 6$ (Verma et al. 2007; Eyles et al. 2007; Stark et al. 2007; Yabe et al. 2009; Stark et al. 2009). These various studies selected LBGs in different ranges of luminosity, using different colour selections, and obtained results which appear in conflict in some cases. However, all of them estimated stellar masses *photometrically*, by fitting models for galaxy SEDs (with an assumed IMF) to flux measurements at different wavelengths ranging, in the rest frame, from the far-UV to the optical. These SED models depend on a significant number of parameters in addition to the stellar mass, including dust extinction, age, star formation history and metallicity (and possibly redshift). In principle, all of these parameters should be determined simultaneously from the SED-fitting. In practice, this leads to degeneracies between different parameters, and significant uncertainties in the stellar masses, by factors up to 10 (e.g. Papovich et al. 2001; Verma et al. 2007; Yabe et al. 2009). These studies all used a Salpeter or other similar Solar neighbourhood IMF. If one allows larger variations in the IMF (as assumed in our model), then the uncertainties in the estimated stellar masses become even larger. Since the top-heavy IMF plays an important role in our model, it is not meaningful to compare stellar masses from the model directly with observational estimates which assume a Salpeter or similar IMF. Therefore we do not make a detailed comparison with values of stellar mass estimated from observational data, but simply note a few numbers. Papovich et al. (2001) and Shapley et al. (2001) find typical stellar masses $\sim 10^{10} M_\odot$ for LBGs at $z = 3$ with $M_{\rm AB}(1500\text{Å}) - 5 \log h \sim -20$. Verma et al. (2007) find masses $\sim 2 \times 10^9 M_\odot$ for similar luminosities at $z = 5$. For LBGs at $z = 4 - 6$, Stark et al. (2009) find stellar masses $\sim 10^9 - 10^{10} M_\odot$ over the luminosity range $-19 \lesssim M_{\rm AB}(1500\text{Å}) - 5 \log h \lesssim -21$, with only a weak dependence on redshift at a given luminosity. Our model predicts values of the stellar mass which are ~ 30 times smaller at a given luminosity and redshift.

However, the observational estimates of stellar mass are driven mainly by the fluxes measured at rest-frame optical wavelengths, so given the effects of the IMF, it is more meaningful to compare directly with these flux measurements. As an example, in Fig. 12 we compare our model predictions with the *Spitzer* 3.6μm fluxes measured by Stark et al. (2009) for LBGs at $z = 4 - 6$ as a function of the optical flux. We have chosen the Stark et al. sample because it is large, homogeneously selected, and covers a wider range of redshift and luminosity than other studies. At the redshifts of these galaxies, the 3.6μm band corresponds to a rest-frame wavelength of $5000 - 7000\text{Å}$, while the *i*- or *z*-band optical magnitude corresponds to $1200 - 1600\text{Å}$ in the rest frame. In the Figure, the lines show the medians predicted by the model, while the filled circles show the median values of 3.6μm magnitude measured by Stark et al.. The predicted relation is seen to lie 0.8-1.6 mag (i.e. a factor 2-4) fainter in the 3.6 μm magnitude than the observations. The discrepancy is thus ~ 10 times smaller than the apparent discrepancy in stellar masses, confirming that the latter is mostly due to the difference between the IMF in the model and the IMF assumed in the observational estimates of stellar mass. Interestingly, the model predicts a very similar trend of rest-frame optical vs. far-UV luminosity as seen in the observational data, with almost no dependence on redshift in the range $z = 4 - 6$. The weak dependence on redshift in the model presumably results from the LBGs mostly being starbursts. We will make a more detailed comparison of the predicted rest-frame far-UV to optical SEDs of LBGs with observations in a future paper.

4.3 Burst fraction

The top right panel of Fig. 11 shows the fraction of galaxies which are currently undergoing a burst. The burst population dominates at higher luminosities and higher redshifts, with a transition to more quiescent systems at lower luminosities. This is important for understanding many of the other properties. In the Baugh05 model, bursts are triggered only by galaxy mergers. As discussed in §3.2.2, the bursts responsible for LBGs in the model are typically triggered by minor, rather than major, galaxy mergers. The burst e-folding timescale varies over the range $\sim 0.01 - 0.2\,\text{Gyr}$ for model LBGs in the luminosity range shown here, for $z = 3 - 10$. It typically increases with luminosity but decreases with increasing redshift. Note that the burst e-folding time can be significantly shorter than the burst SFR timescale due to the effect of supernova feedback. Bursts are assumed to last for 3 e-folding times in our fiducial model. However, the brightest LBGs are on average seen only a small fraction of an e-folding time after the burst began - this is presumably a selection effect due to a burst being brightest in its early stages when the SFR is highest.

4.4 Halo masses and clustering bias

Dark halo masses are shown in the middle left panel of Fig. 11. The trends with luminosity and redshift are similar to those already discussed for the stellar mass. They also cover a wide range, from $\sim 10^{12} h^{-1} M_\odot$ at the highest luminosities and lower redshifts, down to $\sim 10^9 h^{-1} M_\odot$ or less at low luminosities and high redshifts.

The masses of the dark halos hosting LBGs are not directly observable, but they can be constrained from clustering measurements. In the middle right panel of Fig. 11, we show the predicted mean large-scale clustering bias of LBGs. We calculated this using the analytical halo bias formula of Sheth et al. (2001), averaging the bias over the distribution of host halo masses in each bin or range of luminosity (see Baugh et al. 1998 for details). This bias applies on scales larger than roughly the sum of the virial radii of the two host halos. The solid lines show the mean bias within a luminosity bin, while the dashed lines show the mean bias for galaxies brighter than a given luminosity. The bias increases with increasing redshift, and also generally with increasing luminosity, although the latter dependence is weak at lower redshifts. A similar behaviour for bias of LAEs in the same model was earlier found by Orsi et al. (2008). We predict a bias $b \sim 2$ at $z = 3$, nearly independent of luminosity, increasing to $b \sim 4 - 7$ at $z = 10$ and to $b \sim 8$ at $z = 15$. This increase of the bias with redshift reflects the fact that selecting at a fixed luminosity picks out host halos further and further out on the tail of the halo mass function at larger and larger redshifts, which are more and more strongly clustered relative to the dark matter as a whole.

Observational measurements of clustering of LBGs include those of Adelberger et al. (1998) and Giavalisco et al. (1998) at $z = 3$ and Ouchi et al. (2004) at $z = 4 - 5$. Ouchi et al. combine their own and previous clustering measurements with theoretical predictions of the dark matter clustering to estimate $b \approx 2.7 \pm 0.4$ at $z \approx 3$, $b \approx 3.5 \pm 0.7$ at $z \approx 4$ and $b \approx 4.6 \pm 1.1$ at $z \approx 5$ for LBGs with $M_{\rm AB}(1500\text{Å}) - 5 \log h \lesssim -20$. Our model predictions are $b \approx 2.2, 2.8, 3.5$ respectively for the same redshifts and luminosities, which are consistent with these estimates within their errors. We will investigate the clustering in more detail in a future paper.

4.5 Circular velocity

The circular velocity at the stellar half-mass radius is plotted in the lower left panel of Fig. 11. While the trends with luminosity and redshift are qualitatively similar to those for stellar and halo mass, the dependence on redshift is weaker and the total range of values is much smaller, from $\sim 40 \mathrm{km\,s^{-1}}$ at the lowest luminosities and highest redshifts plotted, up to $\sim 250 \mathrm{km\,s^{-1}}$ at the highest luminosities and lowest redshifts. At higher luminosities ($M_{\mathrm{AB}}(1500\mathring{A}) - 5\log h \lesssim -19$), there is almost no dependence of circular velocity on redshift.

The velocity widths of LBGs at $z \sim 3$ have been measured from their rest-frame optical emission lines by Pettini et al. (1998, 2001). These lines (unlike emission and absorption lines in the rest-frame UV) reflect the kinematics of the star-forming gas in the galaxies, which should be related to the rotation velocity of the galaxy. Pettini et al. (2001) measure a median 1-D velocity dispersion $\sigma \approx 70 \mathrm{km\,s^{-1}}$ in LBGs with $M_{\mathrm{AB}}(1500\mathring{A}) - 5\log h \sim -21$. Allowing for inclination and other effects in galaxy disks, this corresponds to a typical circular velocity $V_{\mathrm{c}} \approx 120 \mathrm{km\,s^{-1}}$ (Rix et al. 1997). The line widths measured from CO in two gravitationally-lensed LBGs imply similar values for σ and V_{c} (Baker et al. 2004; Coppin et al. 2007). Our model predicts a median circular velocity $\sim 200 \mathrm{km\,s^{-1}}$ at the same luminosity and redshift, somewhat larger than the observational estimates.

4.6 B/T and morphology

The bottom right panel of Fig. 11 shows the bulge-to-total ratio B/T, either measured in dust-extincted rest-frame 1500$\mathring{A}$ luminosity (solid lines) or in stellar mass (dotted lines). We see that LBGs are very bulge-dominated in their rest-frame UV light at higher luminosities, but with a transition to disk domination at low luminosities. This reflects the dominance of bursts at the higher luminosities, since our model assumes that star formation in bursts all occurs in the bulge component. The dominance of the bulge is generally less extreme in terms of stellar mass. At the highest luminosities, LBGs are predicted to be disk-dominated in stellar mass even though they are bulge-dominated in rest-frame UV light. This reflects the triggering of many starbursts by minor galaxy mergers, which leave the stellar disk of the larger galaxy intact, but sweep all of the cold gas into the bulge, where it forms stars in a burst.

HST imaging has revealed a wide range of morphologies for LBGs. Ravindranath et al. (2006) fit Sersic profiles to the rest-frame far-UV images of a large sample of LBGs at $z = 3 - 5$ with $M_{\mathrm{AB}}(1500\mathring{A}) - 5\log h \lesssim -19.5$. Based on this, they classified about 30% as bulge-dominated, 40% as exponential, and 30% as multiple cores, suggesting galaxy mergers. Lotz et al. (2006) analysed a smaller sample of LBGs at $z \sim 4$ (also in the rest-frame far-UV) using completely different techniques, but arrived at similar conclusions, finding $\sim 30\%$ undisturbed bulgelike morphologies, $\sim 10 - 25\%$ major mergers, and $\sim 50\%$ exponential disks or minor mergers. Our model predicts that most LBGs at these luminosities should be minor and major mergers, with the far-UV light dominated by a bulgelike burst component, which seems qualitatively consistent with the observational results.

4.7 Star formation rates and specific SFRs

We show the SFRs of LBGs in the top left panel of Fig. 13. The solid lines show SFR plotted against dust-extincted far-UV luminosity, and the dotted lines against the unextincted luminosity.

There is an almost linear relation between the SFR and the far-UV luminosity, with the lines for different redshifts lying almost on top of each other. A constant linear relation between rest-frame 1500$\mathring{A}$ luminosity and SFR would be expected under the following conditions: (a) a single IMF dominates; (b) dust extinction is zero or constant; (c) SFR varies on timescales $\gtrsim 10^8 \mathrm{yr}$. In the Baugh05 model, stars form with a top-heavy ($x = 0$) IMF in bursts and a Kennicutt IMF in quiescent disks. For a constant SFR and Solar metallicity, the ratio $L_\nu(1500\mathring{A})/SFR$ is 3.4 times larger for the $x = 0$ IMF than for the Kennicutt IMF (and 2.6 times larger for 0.2 times Solar metallicity). The LBG LF changes from being dominated by bursts at high luminosities to being dominated by quiescent galaxies at low luminosities, and this causes a corresponding shift in the unextincted SFR vs $L_\nu(1500\mathring{A})$ relation, which can be seen for the lower redshifts in the plot. The effects of changes in metallicity with redshift on the unextincted relation seem to be small. Comparing the solid and dotted lines, dust extinction is seen to introduce more scatter into the SFR vs $L_\nu(1500\mathring{A})$ relation, but the average effect of the extinction depends only modestly on luminosity and redshift. Observationally, SFRs of LBGs are generally inferred directly from their rest-frame far-UV luminosities, with or without a correction for dust extinction, so such estimates do not provide an independent test of the relation plotted here. Observational studies typically assume a Salpeter IMF over the mass range $0.1 - 100 M_\odot$ for converting luminosities to SFRs. This Salpeter IMF would require an SFR 4.6 times larger than our top-heavy burst IMF to produce the same unextincted far-UV luminosity (for a constant SFR and Solar metallicity).

The top right panel of Fig. 13 shows the specific star formation rate (SSFR), defined here as the ratio of the current SFR to the stellar mass. There is a strong increase of the SSFR with redshift, and a weaker trend with luminosity. LBGs at higher redshifts are thus forming stars at a much larger fractional rate than lower redshift LBGs, by factors up to $\sim 10^3$. The age, $t(z)$, of the universe is, of course, much less at higher redshift (shrinking from 2.1 Gyr at $z = 3$ to 0.26 Gyr at $z = 15$), so it might be more physically meaningful to plot $t(z) \times SFR/M_{star}$. This would still increase by a factor $\sim 10^2$ from $z = 3$ to $z = 15$. Finally, we should account for the fact that the rate of buildup of mass in long-lived stars is actually $(1 - R) \times SFR$, where R is the fraction of the initial stellar mass returned to the ISM by mass loss from dying stars. R has the value 0.41 for the Kennicutt IMF but 0.91 for the top-heavy IMF. So the current rate of buildup of stellar mass compared to the past average rate is $(1-R)t(z)SFR/M_{star}$. Allowing for the shift between burst and quiescent domination with changing luminosity, this latter quantity still increases by a factor ~ 10 over the range $z = 3$ to $z = 15$, with the high-z LBGs having $(1-R)t(z)SFR/M_{star} \sim 10$. Thus, by any reasonable measure, the highest redshift LBGs are predicted to be assembling stars extremely rapidly compared to their past average rate.

4.8 Cold gas masses and gas fractions

The middle left panel of Fig. 13 shows the cold gas masses of LBGs, where by "cold" gas we mean all of the gas which has condensed into the galaxy, as distinct from the "hot" gas which remains distributed in the halo. Most of the cold gas will be in either atomic or molecular form. The brightest LBGs are predicted to have cold gas masses $\sim 10^{10} h^{-1} M_\odot$. At higher luminosities and higher redshifts, there is a very nearly linear relation between the cold gas mass and the dust-extincted far-UV luminosity. This is a consequence of two effects: the nearly linear relation between SFR and
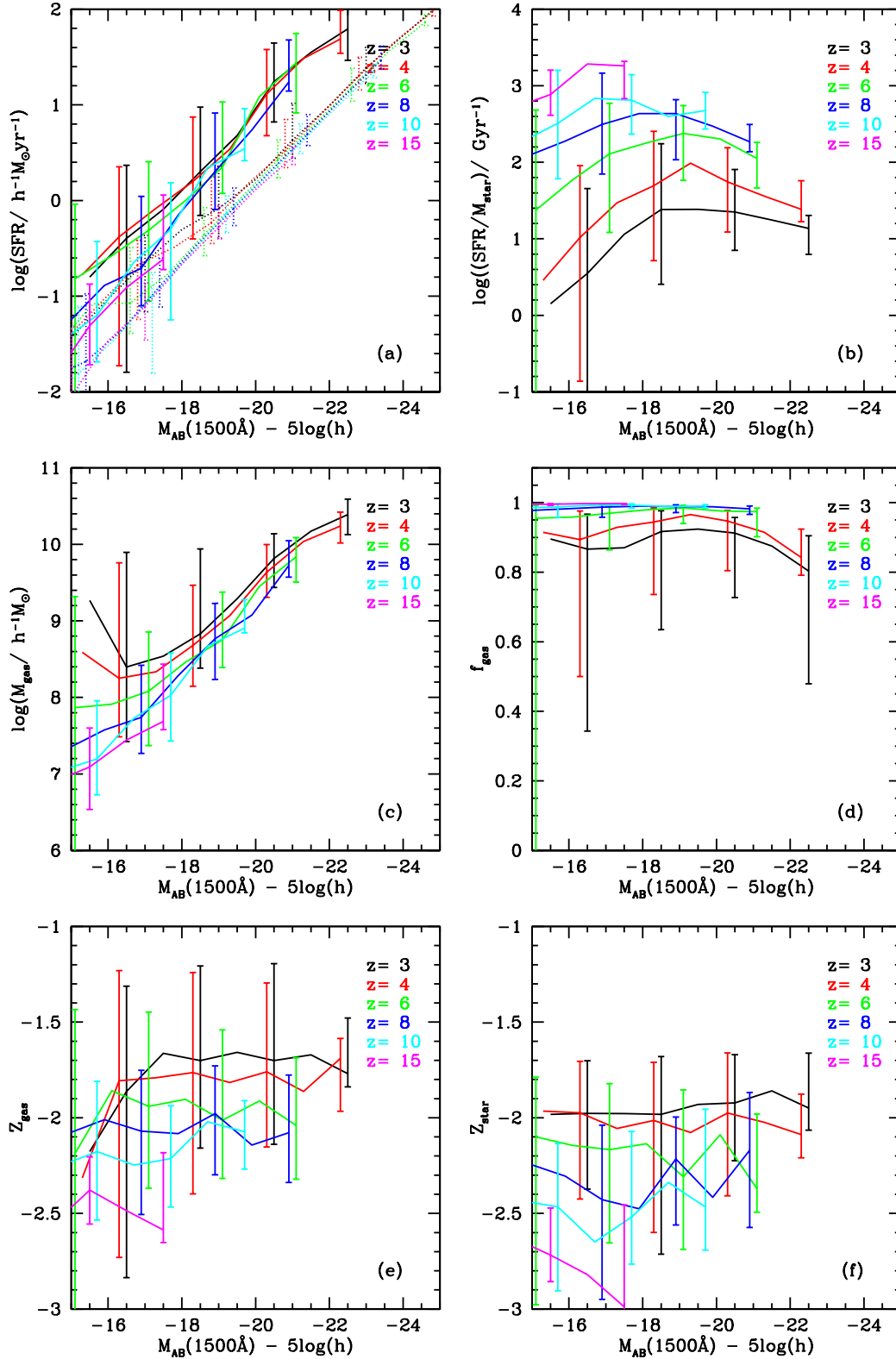
Figure 13. Further predicted physical properties of LBGs as functions of dust-extincted rest-frame 1500Å absolute magnitude in the Baugh05 model. The lines show medians and the error bars indicate the 10-90% range. The different panels are as follows: (a) SFR – the solid and dotted lines show the relations with and without dust extinction in the UV luminosity; (b) specific SFR; (c) cold gas mass; (d) cold gas fraction; (e) gas metallicity; (f) stellar metallicity.

dust-extincted luminosity already noted above, and the fact that the more luminous LBGs are bursts, for which $SFR = M_{\mathrm{gas}}/\tau_*$, with most of the bursts having very similar star formation timescales, τ_*, according to our model. The linear relation between M_{gas} and $L_\nu(1500\text{Å})$ breaks down at low luminosities where quiescent galaxies become important. These have longer SFR timescales than bursts, and so must have more gas to produce the same far-UV luminosity from young stars.

The middle right panel of Fig. 13 shows the gas fractions in LBGs, where we define this fraction as the ratio of cold gas mass to total cold gas + stellar mass in a galaxy. Although the gas fraction shows a very large scatter at lower luminosities, the median value is predicted to be very high $\sim 90 - 99\%$. This results from two effects in the model: the SFR timescale in disks is large compared to the age of the universe at high-z, so that these disks are gas-rich, and most of the bursts are triggered by minor mergers, for which we require the gas fraction in the disk of the primary galaxy to exceed 75% for a burst to be triggered.

Molecular gas has been observed through its CO emission in two gravitationally lensed LBGs at $z \sim 3$, both of which have rest-frame luminosities $M_{\mathrm{AB}}(1500\text{Å}) - 5\log h \sim -20$ (Baker et al. 2004; Coppin et al. 2007). The two galaxies have CO luminosities which differ by a factor 7. The conversion from CO luminosity to molecular gas mass is significantly uncertain. Coppin et al. use a conversion factor estimated for local starburst galaxies, and find molecular gas masses of 0.34 and $2.5 \times 10^9 M_\odot$ for the two galaxies. Using instead the conversion factor estimated for the Milky Way would increase these estimated gas masses by a factor ~ 6. Our model predicts a median cold gas mass (including both molecular and atomic gas) $\sim 4 \times 10^9 M_\odot$ at the same luminosity and redshift. This seems compatible with the current observations, given their uncertainties.

4.9 Metallicities of gas and stars

Finally, the bottom left and right panels of Fig. 13 show the metallicities of cold gas and stars respectively (the latter being a mass-weighted mean value over stars of all ages). We see that, at a given redshift and luminosity, the metallicity of the gas is generally somewhat higher than that of the stars for LBGs that are dominated by bursts. This reflects the buildup of gas metallicity by self-enrichment in a current burst, while the stellar metallicity is an average over past activity. For both gas and stars, the metallicities typically depend only weakly on luminosity, and more strongly on redshift, again for the LBGs which are dominated by bursts. However, even at very high redshifts, the metallicities of LBGs are predicted to be non-negligible (e.g. $Z_{\mathrm{gas}} \sim 0.003$ at $z = 15$), due to self-enrichment by bursts which have large heavy element yields due to the top-heavy IMF.

The gas metallicities of $z \sim 3$ LBGs have been estimated by Pettini et al. (2001) from rest-frame optical HII region emission lines, for a sample of 4 LBGs with $M_{\mathrm{AB}}(1500\text{Å}) - 5\log h \sim -21$. They find significant uncertainties in the values for individual galaxies, but they are all constrained to be in the range $\sim 0.1 - 1 Z_\odot$ (where the solar metallicity $Z_\odot = 0.02$), with a preference for somewhat subsolar values. Our model predicts roughly solar metallicities for the gas at this luminosity and redshift, compatible with the upper end of the observed range. The stellar metallicities of LBGs are only very weakly constrained by SED-fitting to observed broadband fluxes, due to degeneracies with other parameters (Papovich et al. 2001), but are compatible with our model predictions.
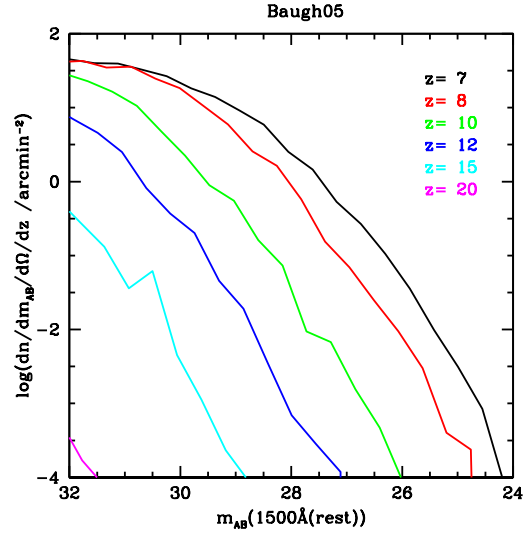
Figure 14. Predicted evolution of the LBG luminosity function at $z = 7 - 20$ in the Baugh05 model, shown as a surface density of objects (number per solid angle per unit redshift) *vs* dust-extincted apparent magnitude at a fixed rest-frame wavelength of 1500Å.

5 PREDICTIONS FOR LBGs AT VERY HIGH REDSHIFTS

In this section, we present additional predictions for LBGs at very high redshifts, $z > 7$, which are starting to be probed with HST, and which in future will be probed to higher redshifts and fainter fluxes by *JWST*, as well as by future 20-40m ELTs on the ground, including the *E-ELT*, *TMT* and *GMT*. NIRCam on *JWST* will do imaging over the wavelength range 0.6-5μm, and so can in principle detect LBGs over the whole redshift range $z = 7 - 20$ and beyond, if they are bright enough and numerous enough. Among the surveys planned with NIRCam are the Deep-Wide Survey (DWS), to reach $m_{\mathrm{AB}} = 30$ over an area of 100 arcmin^2, and the Ultra-Deep Imaging Survey (UDS), to reach $m_{\mathrm{AB}} = 31$ over 10 arcmin^2 (Gardner et al. 2006).

We start by presenting in Fig. 14 predictions from the Baugh05 model for the number of $z > 7$ LBGs, this time shown as the surface density of objects (number per unit redshift per square arcmin) *vs* apparent magnitude. For simplicity, we present results in this section in terms of the apparent magnitude for a fixed rest-frame wavelength of 1500Å, regardless of redshift. In reality, future LBG surveys will use a variety of filters, depending both on the telescope and on the redshift being targetted. However, in order to detect the Lyman-break feature reliably, such surveys will always include at least one filter probing wavelengths close to 1500Å in the rest frame. Predictions for the number of LBGs in any future survey can therefore be approximately read off from Fig. 14, using the apparent magnitude limit for the filter which is closest to rest-frame 1500Å at the target redshift. We see from Fig. 14 that the planned DWS and UDS surveys on *JWST* should each detect a few LBGs at $z = 15$, and many more at lower redshifts. For convenience in what follows, we note that for the cosmology assumed in the Baugh05 model, the relationship between apparent and absolute magnitudes at the same rest-frame wavelength is $m_{\mathrm{AB}} - (M_{\mathrm{AB}} - 5\log h) = (46.16, 46.37, 46.71, 46.97, 47.29, 47.69)$ at the redshifts $z = (7, 8, 10, 12, 15, 20)$ plotted in Figs. 14 and 15. An apparent magnitude $m_{\mathrm{AB}} = 31$ at $z = 15$ thus corresponds to an absolute magnitude $M_{\mathrm{AB}}(1500\text{Å}) - 5\log h = -16.3$.
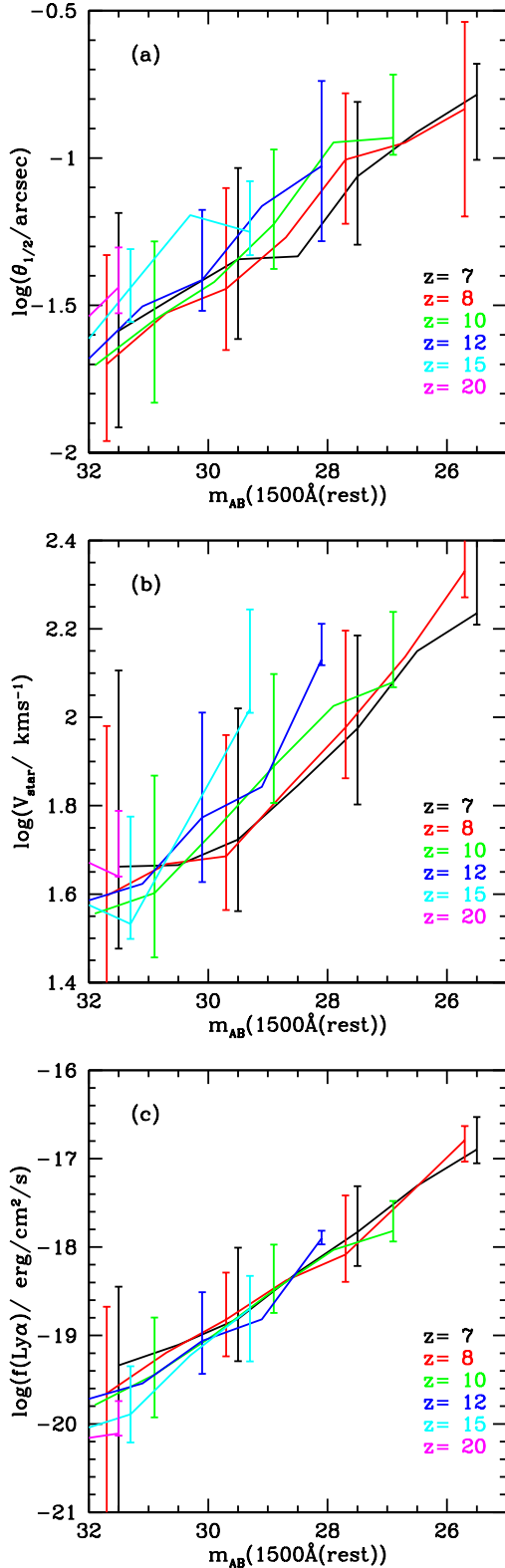
Figure 15. Predicted observable properties of LBGs at $z \geqslant 7$ in the Baugh05 model as functions of dust-extincted apparent magnitude at a fixed rest-frame wavelength of 1500Å. The lines show median values and the error bars show the 10-90% ranges. (a) Angular half-light radius at rest-frame 1500Å. (b) Circular velocity at stellar half-mass radius. (c) $Ly\alpha$ flux (assuming a $Ly\alpha$ escape fraction $f_{esc} = 0.02$).

We next present in Fig. 15 a few directly observable properties of high-z LBGs as functions of rest-frame 1500Å apparent magnitude. These particular properties are chosen because they are directly relevant to the detectability of these LBGs by different instruments on the *JWST* and on future ELTs. The top panel of Fig. 15 shows the angular half-light radius at a rest-frame wavelength of 1500Å. This shows that at a given apparent magnitude, LBGs have slightly larger angular sizes at higher redshifts. This reversal of the trend seen for proper size vs absolute magnitude shown in Fig. 10 is due to the combined effects of angular diameter and luminosity distances. LBGs at $m_{AB} = 30$ and $z = 15$ are predicted to have angular radii ~ 0.05 arcsec, close to the diffraction limit of *JWST* at the relevant wavelength. The middle panel shows the predicted circular velocity at the stellar half-mass radius. This affects the widths of emission and absorption features in a galaxy spectrum, and so is relevant for spectroscopic studies. The dependence of circular velocity on apparent magnitude and redshift is again modest, varying from $\sim 40\,\mathrm{km\,s^{-1}}$ to $\sim 150\,\mathrm{km\,s^{-1}}$ over the whole range plotted. At a fixed apparent magnitude, LBGs have larger circular velocities at high redshift.

Finally, in the bottom panel we show the predicted $Ly\alpha$ line flux. This depends on the fraction of $Ly\alpha$ photons which escape from galaxies, which is very difficult to calculate from first principles due to the effects of resonant scattering of $Ly\alpha$ by atomic hydrogen. We therefore follow the same approach as in our previous work on $Ly\alpha$ emitters using GALFORM, and assume a constant escape fraction, tuned to match observations at lower redshifts. Le Delliou et al. (2006) and Orsi et al. (2008) showed that the observed numbers and properties of $Ly\alpha$ emitters at $z = 3 - 6$ could be reproduced well in the Baugh05 model by assuming a constant escape fraction of 2%, so we use the same value here. We see that LBGs at different redshifts all fall on the same linear relation between $Ly\alpha$ flux and rest-frame far-UV flux. LBGs with $m_{AB} = 30$ are predicted to have $Ly\alpha$ fluxes $\sim 10^{-19}\mathrm{erg\,cm^{-2}s^{-1}}$. This is probably too faint to be detectable with *JWST* but should be within the reach of the *E-ELT*.

6   EVOLUTION OF SFR AND UV LUMINOSITY DENSITIES

The final topic we consider is the cosmic star formation history and how this is traced by the far-UV luminosity density. We show in Fig. 16 the comoving SFR density as a function of redshift for the Baugh05 and Bower06 models (top and bottom panels). The solid blue curves show the total SFR in all galaxies, while the solid green and red curves show the separate contributions from star formation in disks and in bursts.

In the Baugh05 model, the total SFR density peaks at $z \approx 3$, with quiescent galaxies dominating at $z < 2.5$ and bursts dominating above this. Similar results were shown in Baugh et al. (2005) and Lacey et al. (2010b), but there are small differences of detail because of the modified values for the photoionization feedback parameters, z_{reion} and V_{crit}, that we have used in this paper. As discussed in Lacey et al. (2010b), we also find it useful to show the SFR density in massive stars only (dashed lines), which we define as stars with masses $m > 5M_{\odot}$. These stars, which have lifetimes $< 1 \times 10^8$yr, dominate the production of UV radiation. The two IMFs in our model (assumed to cover the stellar mass range $0.15 < m < 120M_{\odot}$) have very different fractions of their initial stellar mass in high mass stars: $f(m > 5M_{\odot}) = 0.24$ for the Kennicutt IMF assumed for quiescent star formation, and
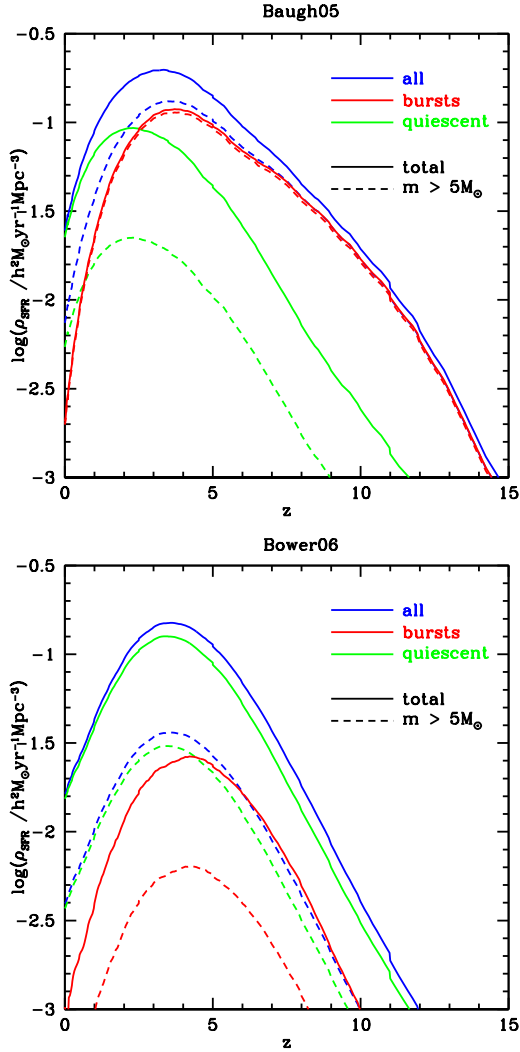
Figure 16. Comoving SFR density *vs* redshift in the Baugh05 and Bower06 models (top and bottom panels). In each panel, the blue line shows the total, while the green and red lines show the separate contributions of disks and bursts. The solid lines show total SFRs integrated over all stellar masses, while the dashed lines show the SFRs in high-mass ($m > 5M_\odot$) stars only.

$f(m > 5M_\odot) = 0.96$ for the top-heavy IMF assumed for bursts. The SFR density for massive stars evolves more strongly than that for all stars, increasing by a factor ≈ 20 from $z = 0$ to its peak at $z \approx 3$, and then declining by a factor ≈ 100 to $z = 15$.

In the Bower06 model, the total SFR density peaks at almost the same redshift as in the Baugh05 model, though at a slightly lower value. However, unlike in the Baugh05 model, the SFR density is dominated by quiescent star formation at all redshifts, and it also drops off more steeply with redshift beyond the peak. The SFR density for massive ($m > 5M_\odot$) stars in the Bower06 model is roughly a factor 3 lower than in the Baugh05 model for $z < 5$, but this difference increases at higher redshifts, reaching a factor ~ 20 at $z = 10$.

In Fig. 17, we show the predicted evolution of the rest-frame 1500Å emissivity (i.e. luminosity density), for the Baugh05 model only. In the left panel, we show the luminosity densities with and without dust extinction (solid and dashed lines), and also show the separate contributions of quiescent and bursting galaxies to the to-

tal. Dust extinction has a large effect on the far-UV emissivity, with the mean extinction (defined from the ratio of emissivities with and without dust) increasing from ≈ 1 mag at $z = 0$ to ≈ 2 mag at $z = 3 - 15$. The mean extinction in the bursts is larger than that in quiescent galaxies at most redshifts, but at $z \gtrsim 1$, the bursts dominate the far-UV emissivity with or without dust extinction. As expected, the unextincted far-UV emissivity approximately tracks the SFR density in high-mass stars shown in Fig. 16 (although changes in the metallicity and in the mix of the IMFs with redshift mean that the scaling is not exact). For comparison, in the Bower06 model, the unextincted far-UV emissivity is below that for the Baugh05 model at all redshifts. However, the mean dust extinction is also lower, peaking at ≈ 1 mag at $z \sim 3$, and falling to ≈ 0.3 mag at $z = 10$. As a result, the extincted emissivity is similar to the Baugh05 model at $z \lesssim 7$, but falls below it at higher redshifts.

In the right panel of Fig. 17, we show the contributions to the dust-extincted 1500Å emissivity from galaxies with rest-frame 1500Å absolute magnitudes brighter than $M_{AB}(1500Å) - 5\log h = -14, -16$ or -18, again for the Baugh05 model. An LBG survey reaching down to $M_{AB}(1500Å) - 5\log h < -18$ (the typical limit for current surveys at $z \gtrsim 7$) will detect the galaxies responsible for 50% of the far-UV emissivity at $z = 5$, but only 5% at $z = 10$. Detecting 80% of the far-UV emissivity at $z = 10$ requires detecting galaxies down to $M_{AB}(1500Å) - 5\log h < -14$, corresponding to an apparent magnitude $m_{AB} \approx 33$ at the same rest-frame wavelength.

Finally, we consider the production of hydrogen-ionizing Lyman continuum (Lyc) photons, which is of critical importance for reionizing the IGM. Fig. 18 shows the evolution of the Lyc emissivity from galaxies predicted by the Baugh05 model. We plot the emissivity without applying any correction for absorption of Lyc photons by dust or gas in the galaxies, (*i.e.* assuming an escape fraction of 100%). The actual escape fraction is probably dominated by absorption on neutral hydrogen, but is currently very uncertain both theoretically and observationally (e.g. Loeb & Barkana 2001; Benson et al. 2006; Shapley et al. 2006). The left panel shows the Lyc emissivities of quiescent and bursting galaxies as green and red lines, with the total in blue. The Lyc emissivity is even more dominated by bursts than is the 1500Å emissivity (at least if absorption by dust and gas are ignored). Bursts dominate at all redshifts $z > 0.2$, and the ionizing emissivity of bursts is 7–50 times larger than that of quiescent galaxies over the whole range $z = 3 - 15$. The reason for this is that stars formed with the top-heavy $x = 0$ IMF produce 11 times more Lyc photons per unit mass of stars formed than the Kennicutt IMF (for Solar metallicity). For comparison, the ratio is only 3.4 for production of 1500Å photons. The right panel shows the contributions to the Lyc emissivity from galaxies brighter than various absolute magnitude limits in dust-extincted 1500Å light. For example, galaxies brighter than $M_{AB}(1500Å) - 5\log h < -18$ are predicted to emit 40% of the hydrogen-ionizing photons at $z = 5$, but only 3% at $z = 10$. Resolving 80% of the ionizing emissivity at $z = 10$ requires detecting galaxies down to $M_{AB}(1500Å) - 5\log h < -14$ (corresponding to $m_{AB} \approx 33$), as for the 1500Å emissivity.

In the Bower06 model, ionizing emissivities are $\sim 7 - 40$ times lower than in the Baugh05 model over the redshift range $z = 3 - 10$ (assuming a 100% escape fraction in both cases). Raičević et al. (2010a) have made a more detailed comparison of the emissivities in these two models.

Benson et al. (2006) investigated reionization in the Baugh05 and other GALFORM models using an analytical Stromgren sphere model for the growth of ionized regions in the IGM, and found that
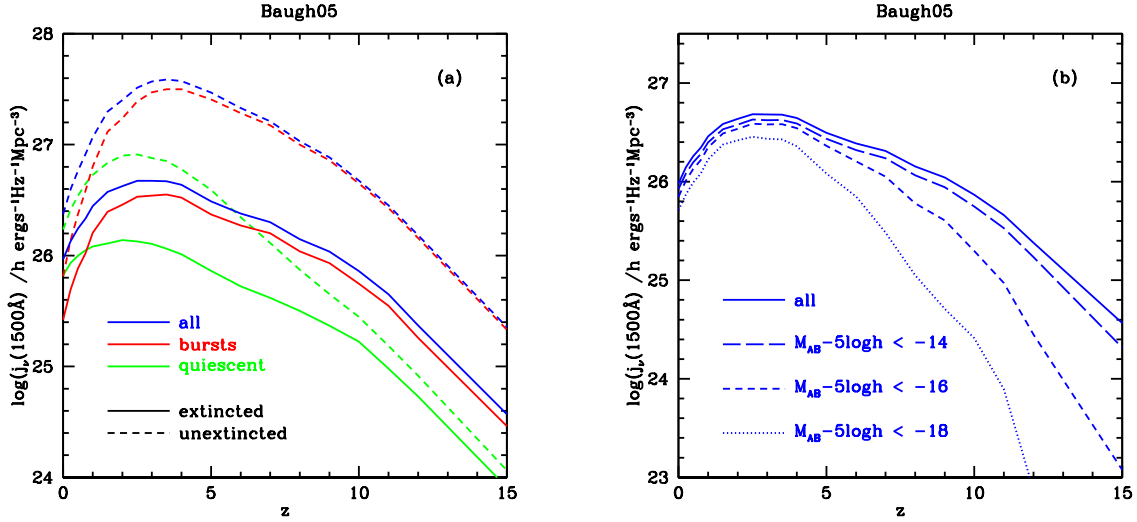
Figure 17. Rest-frame 1500Å luminosity density (in comoving units) *vs* redshift in the Baugh05 model. (a) The blue lines show the far-UV luminosity density due to all galaxies, while the green and red curves show the separate contributions of quiescent galaxies and ongoing bursts. Solid and dashed curves show luminosity densities with and without dust extinction. (b) The contribution to the dust-extincted far-UV luminosity density from galaxies with 1500Å luminosities brighter than different limits, as indicated in the key.
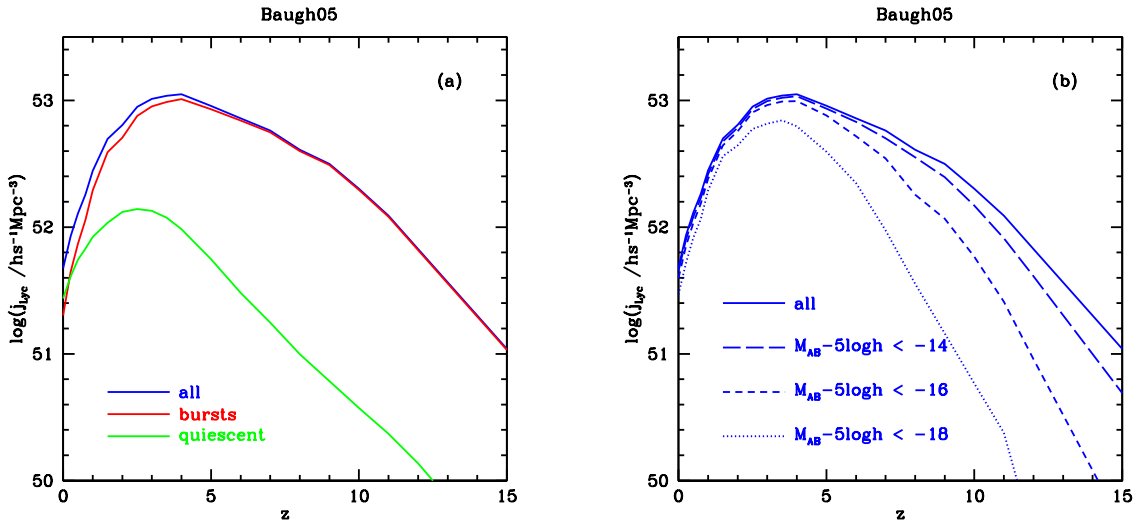

Figure 18. Ionizing emissivity (number of Lyc photons per unit time per unit comoving volume) *vs* redshift in the Baugh05 model. (a) The blue curve shows the total emissivity (without dust extinction) and the green and red curves show the separate contributions of quiescent galaxies and ongoing bursts. (b) The contribution to the ionizing emissivity from galaxies with 1500Å luminosities brighter than different limits, as indicated in the key.

reionization was predicted to occur at $z \approx 12$ for a Lyc escape fraction of 100%. Reionization in this model is studied in much greater detail in Raičević et al. (2010a,b), who use a radiative transfer simulation to show that, for a Lyc escape fraction in the range 0.1–1, reionization should occur at $z \approx 8 - 10$.

7   CONCLUSIONS

We have made a detailed investigation of the properties and evolution of Lyman-break galaxies (LBGs) predicted by hierarchical models of galaxy formation. We followed the galaxy formation process in the framework of the ΛCDM cosmology using the GALFORM semi-analytical model, which includes physical treatments of the hierarchical assembly of dark matter halos, shock-

heating and cooling of gas, star formation, feedback from supernova explosions, AGN and photoionization of the IGM, galaxy mergers and chemical enrichment. The luminosities of galaxies are calculated from a stellar population synthesis model, and dust extinction is then included using a self-consistent theoretical model based on the results of radiative transfer calculations. The dust mass is calculated from the predicted mass and metallicity of the cold gas component, and this is combined with the predicted galaxy radius to calculate the dust extinction optical depth. The far-UV dust extinction is a critical component in any model for LBGs.

We have presented predictions for two variants of the GALFORM model. In the Baugh et al. (2005, Baugh05) model, the formation of very massive galaxies is inhibited by supernova-driven superwinds which eject gas from halos, star formation at high redshifts is dominated by starbursts triggered by galaxy mergers, and

stars form in these bursts with a top-heavy IMF. The top-heavy IMF was motivated by the need to explain the number counts and redshift distributions of the faint sub-mm galaxies. This model also matches a wide range of other data on local galaxies (such as gas masses and disk sizes). In the Bower et al. (2006, Bower06) model, the formation of very massive galaxies is instead inhibited by AGN feedback which heats the gas in halos, starbursts play a much smaller role in star formation, and all stars form with a Solar neighbourhood IMF. The Bower06 model underpredicts the sub-mm number counts by more than an order of magnitude, due to having too few very luminous and dusty star-forming galaxies at high redshifts. This shortcoming might be remedied by introducing a top-heavy IMF in bursts, as we will explore in a future paper. Both models match the present-day optical and near-IR luminosity functions.

We first considered the evolution of the rest-frame far-UV luminosity function (§3). Both models predict modest evolution over the redshift range $3 \lesssim z \lesssim 8$, but a more rapid evolution at higher redshifts, $z \gtrsim 8$, driven by the build-up of dark matter halos. However, the models differ in that the Bower06 model predicts a more extended high-luminosity tail than the Baugh05 model, once dust extinction is included. The effects of dust extinction on the far-UV luminosity function are much larger in the Baugh05 model (~ 2 mag) because the bright end of the luminosity function is dominated by starbursts in which the dust content is enhanced by metal production with the top-heavy IMF. We made a detailed comparison of the predictions of both models with observed far-UV luminosity functions of LBGs over the redshift range $z = 3 - 10$. We found that the Baugh05 model, without any modification of its parameters, predicts a far-UV luminosity function in excellent agreement with current observational data over this whole range. On the other hand, the Bower06 model conflicts with the LBG observations at $z = 3 - 7$ because it predicts too many high-luminosity galaxies. We then investigated the effect on the predicted luminosity functions of varying some of the model parameters from their default values. Assuming a Solar neighbourhood, rather than top-heavy, IMF in bursts has only a modest impact on the far-UV luminosity function, because the effects of lower intrinsic stellar luminosities are partly compensated by lower dust extinctions. However, such a model predicts far too few sub-mm galaxies. We find that the luminosity function over the range covered by observational data is fairly sensitive to the assumed star formation timescale in bursts, especially at higher redshifts, but is less sensitive to the strength of supernova feedback, when these parameters are varied over physically reasonable ranges. The inability of the Bower06 model to match the observed LBG luminosity function data appears to be caused mainly by the short assumed star formation timescale in bursts, rather than by the AGN feedback model or the assumed IMF.

We next investigated a wide range of other physical properties of LBGs predicted by the models (§4). We first considered the sizes of galaxies in the rest-frame far-UV, and compared to recent observational measurements at $z \sim 2 - 7$. We found that both models predicted sizes in reasonable agreement with observations at higher UV luminosities, but only the Baugh05 model is consistent with observed sizes at lower luminosities. We then presented predictions of the Baugh05 model for stellar, halo and gas masses, clustering bias, circular velocity, burst fractions, bulge-to-disk ratios, star formation rates and gas and stellar metallicities, and made brief comparisons with relevant observational data. The model predictions appear to be broadly compatible with current observational constraints (many of which are rather uncertain) in most cases. A

particularly interesting issue is the stellar masses - our predicted values are well below observational estimates based on fitting stellar population models to broad-band photometry. However, the observational estimates all assume a Solar neighbourhood IMF, while in the Baugh05 model the LBG population is dominated by starbursts forming stars with a top-heavy IMF. The observationally inferred stellar masses therefore cannot be directly compared with the values from the model. When instead we compare the IR fluxes (which drive the observational stellar mass estimates) directly, the model is much closer to the observations. We will investigate this important issue in more detail in a future paper. We will also make a more detailed study of LBG clustering in future work, since this provides constraints on the masses of the dark matter halos hosting LBGs.

In §5, we showed predictions for LBGs at very high redshifts ($z = 7 - 20$) in the Baugh05 model, including surface densities of objects down to very faint apparent magnitudes ($m_{AB} = 32$), relevant for observations with future telescopes such as *JWST* and ELTs. We find that deep surveys planned with *JWST* should be able to detect a few LBGs at $z \sim 15$ and $m_{AB} \sim 30 - 31$, and many more at lower redshifts. LBGs detected at $m_{AB} \sim 31$ are predicted to have angular radii $\sim 0.02 - 0.05$ arcsec, depending only weakly on redshift over this range, and to have circular velocities $\sim 30 - 100 \mathrm{km\,s^{-1}}$, again only weakly dependent on redshift.

In §6, we showed the predicted evolution of the far-UV luminosity density, and its relation to the cosmic SFR history, again in the Baugh05 model. The unextincted 1500Å luminosity density tracks the SFR density in high-mass stars ($m \gtrsim 5 M_\odot$) more closely than the total SFR density, since the relative contributions of quiescent and burst star formation (with Solar neighbourhood and top-heavy IMFs respectively) change with redshift. The effect of dust extinction on the far-UV luminosity density is predicted to be large, ≈ 2 mag at 1500Å in the range $3 \lesssim z \lesssim 15$, dropping to ≈ 1 mag at $z = 0$. Finally, we considered the predicted contribution of galaxies to the emissivity of ionizing photons which can reionize the IGM. For a constant escape fraction of ionizing photons from galaxies, this emissivity falls by a factor ~ 100 from its peak at $z \sim 5$ to $z = 15$. At high redshift, most of the ionizing photons are predicted to come from very low luminosity galaxies, so that, for example, to detect the galaxies responsible for $> 50\%$ of the ionizing emissivity at $z = 10$ would require an LBG survey probing fainter than $M_{AB}(1500\text{Å}) - 5 \log h \sim -15$, corresponding to an apparent magnitude $m_{AB} \sim 32$ at the same rest-frame wavelength. The predictions of our model for reionization of the IGM are discussed in much greater detail in Raičević et al. (2010a,b).

In conclusion, we find that the Baugh et al. (2005) model, which was originally constructed to match the far-UV luminosity function of LBGs only at $z = 3$, predicts results in remarkably good agreement with subsequent observations of LBGs out to $z = 10$. Further exploration of whether this model provides a physically accurate description of LBGs and other high-redshift galaxy populations will require more detailed comparisons between the model predictions and observational data (e.g. for stellar masses, clustering, and colours), but also new and more sensitive observations.

REFERENCES

Adelberger K. L., Steidel C. C., Giavalisco M., Dickinson M., Pettini M., Kellogg M., 1998, ApJ, 505, 18

Almeida C., Baugh C. M., Lacey C. G., 2007, MNRAS, 376, 1711

Almeida C., Baugh C. M., Wake D. A., Lacey C. G., Benson A. J., Bower R. G., Pimbblet K., 2008, MNRAS, 386, 2145

Arnouts S., Schiminovich D., Ilbert O., Tresse L., Milliard B., Treyer M., Bardelli S., Budavari et al., 2005, ApJ, 619, L43

Baker A. J., Tacconi L. J., Genzel R., Lehnert M. D., Lutz D., 2004, ApJ, 604, 125

Baugh C. M., 2006, Reports on Progress in Physics, 69, 3101

Baugh C. M., Cole S., Frenk C. S., Lacey C. G., 1998, ApJ, 498, 504

Baugh C. M., Lacey C. G., Frenk C. S., Granato G. L., Silva L., Bressan A., Benson A. J., Cole S., 2005, MNRAS, 356, 1191

Becker R. H., Fan X., White R. L., Strauss M. A., Narayanan V. K., Lupton R. H., Gunn J. E., Annis et al., 2001, AJ, 122, 2850

Bell E. F., 2002, ApJ, 577, 150

Benson A. J., Bower R. G., Frenk C. S., Lacey C. G., Baugh C. M., Cole S., 2003, ApJ, 599, 38

Benson A. J., Lacey C. G., Baugh C. M., Cole S., Frenk C. S., 2002, MNRAS, 333, 156

Benson A. J., Sugiyama N., Nusser A., Lacey C. G., 2006, MNRAS, 369, 1055

Bouwens R. J., Illingworth G. D., Blakeslee J. P., Broadhurst T. J., Franx M., 2004a, ApJ, 611, L1

Bouwens R. J., Illingworth G. D., Franx M., Chary R., Meurer G. R., Conselice C. J., Ford H., Giavalisco M., van Dokkum P., 2009a, ApJ, 705, 936

Bouwens R. J., Illingworth G. D., Franx M., Ford H., 2007, ApJ, 670, 928

Bouwens R. J., Illingworth G. D., Labbe I., Oesch P. A., Carollo M., Trenti M., van Dokkum P. G., Franx M., Stiavelli M., Gonzalez V., Magee D., 2009b, ArXiv e-prints

Bouwens R. J., Illingworth G. D., Oesch P. A., Stiavelli M., van Dokkum P., Trenti M., Magee D., Labbé I., Franx M., Carollo C. M., Gonzalez V., 2010, ApJ, 709, L133

Bouwens R. J., Illingworth G. D., Rosati P., Lidman C., Broadhurst T., Franx M., Ford H. C., Magee et al., 2003, ApJ, 595, 589

Bouwens R. J., Thompson R. I., Illingworth G. D., Franx M., van Dokkum P. G., Fan X., Dickinson M. E., Eisenstein D. J., Rieke M. J., 2004b, ApJ, 616, L79

Bower R. G., Benson A. J., Malbon R., Helly J. C., Frenk C. S., Baugh C. M., Cole S., Lacey C. G., 2006, MNRAS, 370, 645

Buat V., Giovannoli E., Burgarella D., Altieri B., Amblard A., Arumugam V., Aussel H., Babbedge et al., 2010, MNRAS, L119+

Bunker A., Wilkins S., Ellis R., Stark D., Lorenzoni S., Chiu K., Lacy M., Jarvis M., Hickey S., 2009, ArXiv e-prints

Burgarella D., Pérez-González P. G., Tyler K. D., Rieke G. H., Buat V., Takeuchi T. T., Lauger S., Arnouts et al., 2006, A&A, 450, 69

Chapman S. C., Blain A. W., Ivison R. J., Smail I. R., 2003, Nature, 422, 695

Chapman S. C., Scott D., Steidel C. C., Borys C., Halpern M., Morris S. L., Adelberger K. L., Dickinson M., Giavalisco M., Pettini M., 2000, MNRAS, 319, 318

Cole S., Helly J., Frenk C. S., Parkinson H., 2008, MNRAS, 383, 546

Cole S., Lacey C. G., Baugh C. M., Frenk C. S., 2000, MNRAS, 319, 168

Coppin K. E. K., Swinbank A. M., Neri R., Cox P., Smail I., Ellis R. S., Geach J. E., Siana et al., 2007, ApJ, 665, 936

Dunkley J., Komatsu E., Nolta M. R., Spergel D. N., Larson D., Hinshaw G., Page L., Bennett et al., 2009, ApJS, 180, 306

Elmegreen B. G., 2009, in The Evolving ISM in the Milky Way and Nearby Galaxies

Eyles L. P., Bunker A. J., Ellis R. S., Lacy M., Stanway E. R., Stark D. P., Chiu K., 2007, MNRAS, 374, 910

Fan X., White R. L., Davis M., Becker R. H., Strauss M. A., Haiman Z., Schneider D. P., Gregg et al., 2000, AJ, 120, 1167

Fanidakis N., Baugh C. M., Benson A. J., Bower R. G., Cole S., Done C., Frenk C. S., 2010, MNRAS, 1547

Fardal M. A., Katz N., Weinberg D. H., Davé R., 2007, MNRAS, 379, 985

Ferguson H. C., Dickinson M., Giavalisco M., Kretchmer C., Ravindranath S., Idzi R., Taylor E., Conselice et al., 2004, ApJ, 600, L107

Ferrara A., Bianchi S., Cimatti A., Giovanardi C., 1999, ApJS, 123, 437

Figer D. F., Kim S. S., Morris M., Serabyn E., Rich R. M., McLean I. S., 1999, ApJ, 525, 750

Gardner J. P., Mather J. C., Clampin M., Doyon R., Greenhouse M. A., Hammel H. B., Hutchings J. B., Jakobsen et al., 2006, Space Science Reviews, 123, 485

Giavalisco M., Steidel C. C., Adelberger K. L., Dickinson M. E., Pettini M., Kellogg M., 1998, ApJ, 503, 543

Giavalisco M., Steidel C. C., Macchetto F. D., 1996, ApJ, 470, 189

Gnedin N. Y., 2000, ApJ, 542, 535

Gonzalez J. E., Lacey C. G., Baugh C. M., Frenk C. S., 2010a. In preparation

—, 2010b, ArXiv e-prints

González J. E., Lacey C. G., Baugh C. M., Frenk C. S., Benson A. J., 2009, MNRAS, 397, 1254

Gonzalez-Perez V., Baugh C. M., Lacey C. G., Almeida C., 2009, MNRAS, 398, 497

Granato G. L., Lacey C. G., Silva L., Bressan A., Baugh C. M., Cole S., Frenk C. S., 2000, ApJ, 542, 710

Guo Q., White S. D. M., 2009, MNRAS, 396, 39

Harayama Y., Eisenhauer F., Martins F., 2008, ApJ, 675, 1319

Heckman T. M., Armus L., Miley G. K., 1990, ApJS, 74, 833

Helly J. C., Cole S., Frenk C. S., Baugh C. M., Benson A., Lacey C., 2003, MNRAS, 338, 903

Hoeft M., Yepes G., Gottlöber S., Springel V., 2006, MNRAS, 371, 401

Hu E. M., Cowie L. L., McMahon R. G., 1998, ApJ, 502, L99+

Hughes D. H., Serjeant S., Dunlop J., Rowan-Robinson M., Blain A., Mann R. G., Ivison R., Peacock et al., 1998, Nature, 394, 241

Iwata I., Ohta K., Tamura N., Akiyama M., Aoki K., Ando M., Kiuchi G., Sawicki M., 2007, MNRAS, 376, 1557

Kennicutt Jr. R. C., 1983, ApJ, 272, 54

Lacey C. G., Baugh C. M., Frenk C. S., 2010a. In preparation

Lacey C. G., Baugh C. M., Frenk C. S., Benson A. J., Orsi A., Silva L., Granato G. L., Bressan A., 2010b, MNRAS, 443

Lacey C. G., Baugh C. M., Frenk C. S., Silva L., Granato G. L.,

Bressan A., 2008, MNRAS, 385, 1155

Larson R. B., 1998, MNRAS, 301, 569

—, 2005, MNRAS, 359, 211

Le Delliou M., Lacey C., Baugh C. M., Guiderdoni B., Bacon R., Courtois H., Sousbie T., Morris S. L., 2005, MNRAS, 357, L11

Le Delliou M., Lacey C. G., Baugh C. M., Morris S. L., 2006, MNRAS, 365, 712

Lo Faro B., Monaco P., Vanzella E., Fontanot F., Silva L., Cristiani S., 2009, MNRAS, 399, 827

Loeb A., Barkana R., 2001, ARA&A, 39, 19

Lotz J. M., Madau P., Giavalisco M., Primack J., Ferguson H. C., 2006, ApJ, 636, 592

Madau P., Ferguson H. C., Dickinson M. E., Giavalisco M., Steidel C. C., Fruchter A., 1996, MNRAS, 283, 1388

Malbon R. K., Baugh C. M., Frenk C. S., Lacey C. G., 2007, MNRAS, 382, 1394

Maness H., Martins F., Trippe S., Genzel R., Graham J. R., Sheehy C., Salaris M., Gillessen et al., 2007, ApJ, 669, 1024

McCrady N., Gilbert A. M., Graham J. R., 2003, ApJ, 596, 240

McLure R. J., Cirasuolo M., Dunlop J. S., Foucaud S., Almaini O., 2009, MNRAS, 395, 2196

McLure R. J., Dunlop J. S., Cirasuolo M., Koekemoer A. M., Sabbi E., Stark D. P., Targett T. A., Ellis R. S., 2010, MNRAS, 126

Meurer G. R., Heckman T. M., Calzetti D., 1999, ApJ, 521, 64

Meurer G. R., Wong O. I., Kim J. H., Hanish D. J., Heckman T. M., Werk J., Bland-Hawthorn J., Dopita et al., 2009, ApJ, 695, 765

Nagamine K., 2002, ApJ, 564, 73

Nagashima M., Lacey C. G., Baugh C. M., Frenk C. S., Cole S., 2005a, MNRAS, 358, 1247

Nagashima M., Lacey C. G., Okamoto T., Baugh C. M., Frenk C. S., Cole S., 2005b, MNRAS, 363, L31

Oesch P. A., Bouwens R. J., Carollo C. M., Illingworth G. D., Trenti M., Stiavelli M., Magee D., Labbé I., Franx M., 2010a, ApJ, 709, L21

Oesch P. A., Bouwens R. J., Illingworth G. D., Carollo C. M., Franx M., Labbé I., Magee D., Stiavelli M., Trenti M., van Dokkum P. G., 2010b, ApJ, 709, L16

Okamoto T., Gao L., Theuns T., 2008, MNRAS, 390, 920

Orsi A., Lacey C. G., Baugh C. M., Infante L., 2008, MNRAS, 391, 1589

Ouchi M., Mobasher B., Shimasaku K., Ferguson H. C., Fall S. M., Ono Y., Kashikawa N., Morokuma et al., 2009, ApJ, 706, 1136

Ouchi M., Shimasaku K., Okamura S., Furusawa H., Kashikawa N., Ota K., Doi M., Hamabe et al., 2004, ApJ, 611, 685

Papovich C., Dickinson M., Ferguson H. C., 2001, ApJ, 559, 620

Parkinson H., Cole S., Helly J., 2008, MNRAS, 383, 557

Parra R., Conway J. E., Diamond P. J., Thrall H., Lonsdale C. J., Lonsdale C. J., Smith H. E., 2007, ApJ, 659, 314

Paumard T., Genzel R., Martins F., Nayakshin S., Beloborodov A. M., Levin Y., Trippe S., Eisenhauer et al., 2006, ApJ, 643, 1011

Pérez-González P. G., Rieke G. H., Villar V., Barro G., Blaylock M., Egami E., Gallego J., Gil de Paz et al., 2008, ApJ, 675, 234

Pettini M., Kellogg M., Steidel C. C., Dickinson M., Adelberger K. L., Giavalisco M., 1998, ApJ, 508, 539

Pettini M., Shapley A. E., Steidel C. C., Cuby J., Dickinson M., Moorwood A. F. M., Adelberger K. L., Giavalisco M., 2001, ApJ, 554, 981

Power C., Baugh C. M., Lacey C. G., 2010, MNRAS, 406, 43

Raičević M., Theuns T., Lacey C., 2010a, ArXiv e-prints

Raičević M., Theuns T., Lacey C. G., 2010b. In preparation

Ravindranath S., Giavalisco M., Ferguson H. C., Conselice C., Katz N., Weinberg M., Lotz J., Dickinson et al., 2006, ApJ, 652, 963

Reddy N. A., Steidel C. C., 2009, ApJ, 692, 778

Rieke G. H., Loken K., Rieke M. J., Tamblyn P., 1993, ApJ, 412, 99

Rix H., Guhathakurta P., Colless M., Ing K., 1997, MNRAS, 285, 779

Sawicki M., Thompson D., 2006, ApJ, 642, 653

Sawicki M., Yee H. K. C., 1998, AJ, 115, 1329

Shapley A. E., Steidel C. C., Adelberger K. L., Dickinson M., Giavalisco M., Pettini M., 2001, ApJ, 562, 95

Shapley A. E., Steidel C. C., Pettini M., Adelberger K. L., 2003, ApJ, 588, 65

Shapley A. E., Steidel C. C., Pettini M., Adelberger K. L., Erb D. K., 2006, ApJ, 651, 688

Sheth R. K., Mo H. J., Tormen G., 2001, MNRAS, 323, 1

Shimasaku K., Ouchi M., Furusawa H., Yoshida M., Kashikawa N., Okamura S., 2005, PASJ, 57, 447

Silva L., Granato G. L., Bressan A., Danese L., 1998, ApJ, 509, 103

Smail I., Ivison R. J., Blain A. W., 1997, ApJ, 490, L5+

Somerville R. S., Primack J. R., Faber S. M., 2001, MNRAS, 320, 504

Springel V., White S. D. M., Jenkins A., Frenk C. S., Yoshida N., Gao L., Navarro J., Thacker et al., 2005, Nature, 435, 629

Stark D. P., Bunker A. J., Ellis R. S., Eyles L. P., Lacy M., 2007, ApJ, 659, 84

Stark D. P., Ellis R. S., Bunker A., Bundy K., Targett T., Benson A., Lacy M., 2009, ApJ, 697, 1493

Steidel C. C., Adelberger K. L., Giavalisco M., Dickinson M., Pettini M., 1999, ApJ, 519, 1

Steidel C. C., Giavalisco M., Pettini M., Dickinson M., Adelberger K. L., 1996, ApJ, 462, L17+

Steidel C. C., Hamilton D., 1992, AJ, 104, 941

Stolte A., Brandner W., Grebel E. K., Lenzen R., Lagrange A.-M., 2005, ApJ, 628, L113

Swinbank A. M., Lacey C. G., Smail I., Baugh C. M., Frenk C. S., Blain A. W., Chapman S. C., Coppin et al., 2008, MNRAS, 391, 420

van Dokkum P. G., 2008, ApJ, 674, 29

Verma A., Lehnert M. D., Förster Schreiber N. M., Bremer M. N., Douglas L., 2007, MNRAS, 377, 1024

Weinberg D. H., Hernquist L., Katz N., 2002, ApJ, 571, 15

Yabe K., Ohta K., Iwata I., Sawicki M., Tamura N., Akiyama M., Aoki K., 2009, ApJ, 693, 507

Yan H., Windhorst R., Hathi N., Cohen S., Ryan R., O'Connell R., McCarthy P., 2009, ArXiv e-prints

Yoshida M., Shimasaku K., Kashikawa N., Ouchi M., Okamura S., Ajiki M., Akiyama M., Ando et al., 2006, ApJ, 653, 988

APPENDIX A: COMPARISON OF THE BAUGH ET AL. AND BOWER ET AL. MODELS

The Baugh05 and Bower06 models were originally constructed with somewhat different aims, and their parameters for star formation, feedback etc were chosen by comparison with different, though partly overlapping, observational datasets. The parameters for both models were constrained to reproduce the ob-

served present-day B- and K-band galaxy luminosity functions. The Baugh05 model was constructed to also match a wide range of other properties of present-day galaxies, including the far-IR (60μm) luminosity function and the dependence of disk size, gas content and metallicity on galaxy luminosity. The Bower06 model did not use any of these present-day properties as constraints in choosing its parameters, but instead aimed to reproduce the general form of the colour-magnitude distribution of galaxies at $z = 0$. In addition, the Baugh05 model was designed to explain the observed number counts and redshift distributions of the faint sub-mm (850μm) galaxies, and the rest-frame far-UV luminosity function of Lyman-break galaxies at $z \approx 3$, while the Bower06 model instead focused on matching the observed evolution of the K-band luminosity function of galaxies at $z \lesssim 2$.

Given these differences, it is not surprising that the two models, although fundamentally quite similar, have different successes and drawbacks, as discussed in subsequent papers. González et al. (2009) compared both models side-by-side with observational data from the SDSS on luminosity functions, colours, morphologies and sizes of present-day galaxies. They found that both models are reasonably consistent with the fraction of early-type galaxies as a function of luminosity, but that the Bower06 model is in better agreement with the distribution of galaxy colours. Further, the Baugh05 model agrees much better with the size-luminosity relation of disk galaxies, but both models have problems explaining the sizes of spheroidal galaxies (as also found by Almeida et al. (2007)). Almeida et al. (2008) found the Bower06 model in better agreement with the luminosity function and correlation function of Luminous Red Galaxies (LRGs) in the SDSS. Power et al. (2010) investigated the cold gas mass functions in both models, and found the Baugh05 model in better agreement with data from the HIPASS 21cm survey of the local universe.

At higher redshifts, the Baugh05 model seems in generally better agreement with observations of actively star-forming galaxies at $z \gtrsim 2$, while the Bower06 model is in better agreement with observations of more passive galaxies at $z \lesssim 2$. Bower et al. (2006) compared the evolution of the K-band luminosity function in both models with observations at $z \leqslant 1.5$, and found that the Baugh05 model predicts somewhat too few high-luminosity galaxies at higher redshifts. The Baugh05 model also predicts much lower number counts for Extremely Red Objects (EROs) than Bower06, with the latter being in much better agreement with observational data (Gonzalez-Perez et al. 2009). However, the Bower06 model predicts number counts of faint sub-mm galaxies which are too low by more than an order of magnitude. The comparison of both models with observations of LBGs is the topic of this paper.